Published July 22, 2013

Loss of BubR1 acetylation causes defects in spindle assembly checkpoint signaling and promotes tumor formation

Inai Park,[1] Hae-ock Lee,[1] Eunhee Choi,[1] Yoo-Kyung Lee,[1] Mi-Sun Kwon,[1] Jaewon Min,[1] Pil-Gu Park,[1] Seonju Lee,[1] Young-Yun Kong,[1] Gyungyub Gong,[2] and Hyunsook Lee[1]

[1]Department of Biological Sciences and Institute of Molecular Biology and Genetics, Seoul National University, Seoul 151-742, Korea
[2]Department of Pathology, Asan Medical Center, University of Ulsan College of Medicine, Seoul 138-736, Korea

BubR1 acetylation is essential in mitosis. Mice heterozygous for the acetylation-deficient *BubR1* allele (*K243R/+*) spontaneously developed tumors with massive chromosome missegregations. *K243R/+* mouse embryonic fibroblasts (MEFs) exhibited a weakened spindle assembly checkpoint (SAC) with shortened mitotic timing. The generation of the SAC signal was intact, as Mad2 localization to the unattached kinetochore (KT) was unaltered; however, because of the premature degradation of K243R-BubR1, the mitotic checkpoint complex disassociated prematurely in the nocodazole-treated condition, suggesting that maintenance of the SAC is compromised. BubR1 acetylation was also required to counteract excessive Aurora B activity at the KT for stable chromosome–spindle attachments. The association of acetylation-deficient BubR1 with PP2A-B56α phosphatase was reduced, and the phosphorylated Ndc80 at the KT was elevated in *K243R/+* MEFs. In relation, there was a marked increase of micronuclei and *p53* mutation was frequently detected in primary tumors of *K243R/+* mice. Collectively, the combined effects of failure in chromosome–spindle attachment and weakened SAC cause genetic instability and cancer in *K243R/+* mice.

Introduction

The climax of mitosis is the poleward separation of sister chromatids into two daughter cells. For genetic integrity, the chromosome separation of the duplicated genome must be precisely controlled. Accurate chromosomal segregation in mitosis is ensured by the spindle assembly checkpoint (SAC), a process that ultimately inhibits anaphase-promoting complex/cyclosome (APC/C), which is the multisubunit E3 ligase responsible for the destruction of cyclin B and securin during mitosis, until all of the chromosomes are attached to microtubule (MT) spindles in a bipolar manner (Lara-Gonzalez et al., 2012).

BubR1 is a core component of the SAC, which constitutes the mitotic checkpoint complex (MCC) with Mad2, Bub3, and Cdc20 (Sudakin et al., 2001). The MCC inhibits APC/C in mitosis (Kim and Yu, 2011). BubR1 is also involved in the regulation of chromosome–spindle attachments (Lampson and Kapoor, 2005). BubR1 binds to KNL1/Blinkin, which constitutes the KMN (KNL1/Mis12/Ndc80) network at kinetochores (KTs), where MTs attach (Kiyomitsu et al., 2007; Bolanos-Garcia et al., 2011). Furthermore, BubR1, when phosphorylated by Plk1, recruits the B56α subunit of PP2A phosphatase to KTs and counteracts the excessive Aurora B activity on the KMN network. This dephosphorylation of the KMN network stabilizes the KT–MT attachment (Suijkerbuijk et al., 2012; Kruse et al., 2013). And, BubR1 binds to centromere-associated protein E (CENP-E; Mao et al., 2003; Guo et al., 2012), a plus end–directed motor that enables the gliding of monoorientated chromosomes along the existing KT fiber (K-fiber) to the cell equator (Kapoor et al., 2006). Therefore, in addition to SAC

I. Park and H.-o. Lee contributed equally to this paper.

Correspondence to Hyunsook Lee: HL212@snu.ac.kr

Abbreviations used in this paper: APC/C, anaphase-promoting complex/cyclosome; CENP-E, centromere-associated protein E; ES, embryonic stem; FRT, flippase recognition target; H&E, hematoxylin and eosin; IP, immunoprecipitation; KT, kinetochore; MCC, mitotic checkpoint complex; MEF, mouse embryonic fibroblast; MT, microtubule; NEBD, nuclear envelope breakdown; PMSCS, premature sister chromatid separations; SAC, spindle assembly checkpoint; SKY, spectral karyotyping; WB, Western blot; WT, wild type.

Supplemental Material can be found at:
http://jcb.rupress.org/content/suppl/2013/07/18/jcb.201210099.DC1.html
Original image data can be found at:
http://jcb-dataviewer.rupress.org/jcb/browse/5805

The Rockefeller University Press $30.00
J. Cell Biol. Vol. 202 No. 2 295–309
www.jcb.org/cgi/doi/10.1083/jcb.201210099

Published July 22, 2013

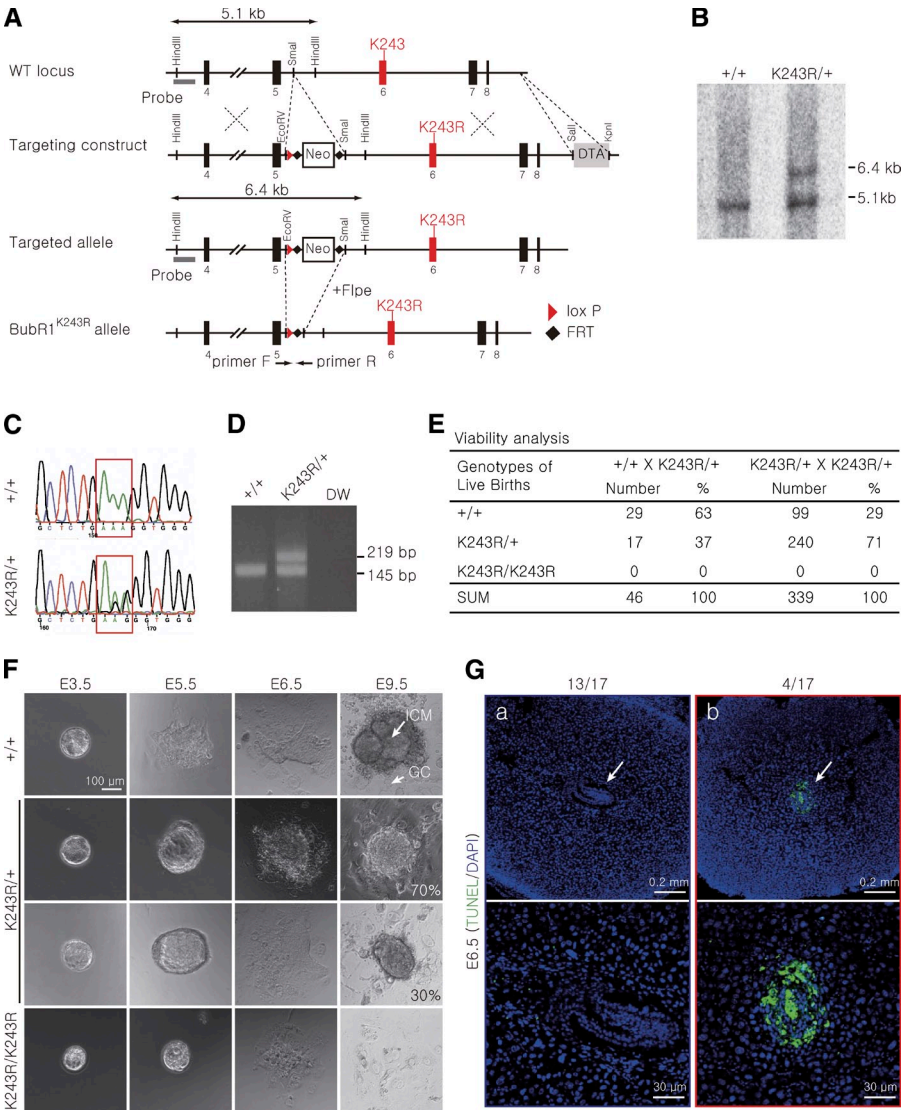

Genotypes of Live Births	+/+ X K243R/+		K243R/+ X K243R/+	
	Number	%	Number	%
+/+	29	63	99	29
K243R/+	17	37	240	71
K243R/K243R	0	0	0	0
SUM	46	100	339	100

Figure 1. **BubR1 acetylation is essential for embryonic development.** (A) Schematic representation of the *BubR1* gene-targeting strategy. Shown are the structures of the WT *BubR1* locus, the targeting construct, the targeted locus, and the disrupted locus after the Flpe-mediated deletion. The neomycin-resistance gene in the targeting construct is removed when crossed with the *Flpe* transgenic mouse to generate the *BubR1*^{K243R} (*K243R*) allele. The probe for Southern blot analysis and the primers for PCR genotyping are marked with gray bars and arrows, respectively. (B) Southern blot analysis of the WT and targeted ES cell lines using the probe indicated in A. HindIII-digested genomic DNA generated a 5.1-kb fragment in the WT and a 6.4-kb band in the targeted allele before the removal of the neo-resistance cassette. (C) Sequence analysis of genomic DNA from WT and *K243R/+* ES cells. (D) Genotyping of WT and *K243R/+* mice using PCR. (E) Summary of the crosses and progeny. The *K243R/+* heterozygous mice were intercrossed, and the newborn pups were scored. (F) In vitro culture of the WT and *K243R/+* embryos. The E3.5 embryos from the *K243R/+* intercrosses were cultured in vitro. The inner cell mass (ICM) and the trophoblast giant cells (GC) are marked. (G) Sagittal sections of the E6.5 embryos in the uterus were examined for apoptosis using TUNEL staining. Low (top) and high (bottom) power magnification images are shown. The arrows indicate embryos or embryonic remnants.

activity, BubR1 function is crucial in chromosome congression, the bipolar spindle attachment that forms the metaphase plate.

We reported previously that BubR1 is acetylated at a single lysine residue, K250, in prometaphase and that acetylated BubR1 inhibits APC/C-Cdc20, whereas deacetylated BubR1 becomes an APC/C substrate (Choi et al., 2009). Furthermore, BubR1 acetylation requires the breast cancer susceptibility gene *BRCA2*, suggesting that BubR1 acetylation is a tumor-suppressive mechanism (Choi et al., 2012).

To elucidate the physiological consequences of BubR1 acetylation, we generated an acetylation-deficient *BubR1* allele (*K243R*) in mice. Here, we report that mice heterozygous for the *K243R* allele are predisposed to various types of cancers and that BubR1 acetylation is required for both SAC maintenance and chromosome congression.

Results

Generation of an acetylation-defective BubR1 allele in mice

We generated an acetylation-defective *BubR1* allele in mice via substitution of the lysine 243 residue, which corresponds to lysine 250 in humans, with an arginine (*K243R*) using knock-in technology (Fig. 1, A–D). We monitored 339 live animals from *BubR1*$^{K243R/+}$ intercrosses and failed to identify any homozygous mutant (*BubR1*$^{K243R/K243R}$) newborn pups. In comparison, the heterozygous mutant mice (*BubR1*$^{K243R/+}$; referred to here as *K243R/+*) survived to birth at the correct Mendelian frequency without apparent developmental defects (Fig. 1 E). Moreover, we did not detect early aging phenotypes, which were observed previously in hypomorphic *BubR1* mice (Baker et al., 2004). *BubR1* expression and the overall protein levels were unaltered in the thymus and testis of the *K243R/+* mice (Fig. S1 A); therefore, these mice differ from *BubR1*-haploinsufficient mice (Wang et al., 2004) and hypomorphic *BubR1* mice (Baker et al., 2004). The body weights and growth rates of the heterozygous mice were comparable to those of wild-type (WT) mice (Fig. S1 B).

To determine when *BubR1*$^{K243R/K243R}$ embryos die, 20 blastocysts at E3.5 from four *K243R/+* intercrosses were subjected to in vitro culture and monitoring (Fig. 1 F). After 3 d, the WT embryos in culture (n = 4) were able to hatch, the trophoblast giant cells spread out in the culture dish, and the inner cell mass was well formed. Out of twelve heterozygous *K243R/+* embryos, eight of them proliferated and exhibited a morphology

Published July 22, 2013

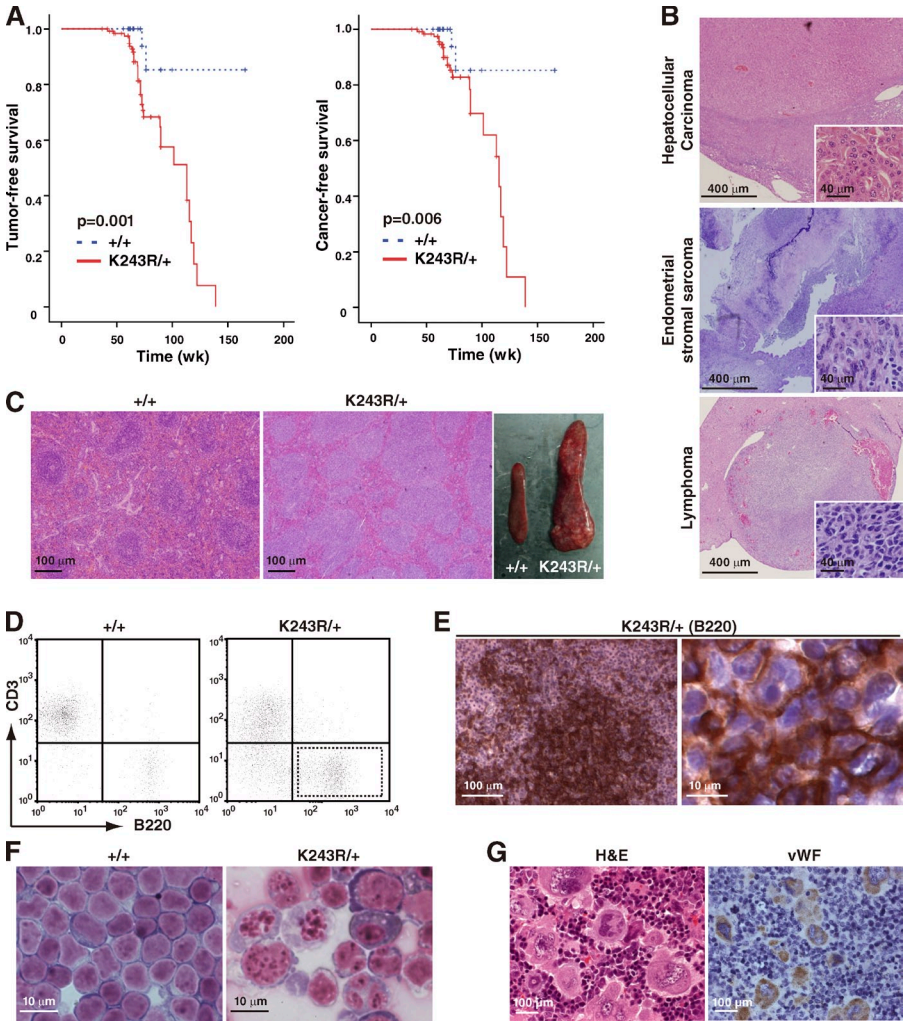

Figure 2. **Spontaneous tumorigenesis in *K243R/+* mice.** (A) Tumor incidence was assessed using Kaplan-Meier graphs. The tumor-free survival analysis (left) includes both benign and malignant tumors; the cancer-free survival analysis (right) includes only the malignant cancers. The statistical analyses were performed using SPSS software. Total number of mice analyzed cumulatively: WT, n = 41; *K243R/+*, n = 121. (B) Representative H&E-stained sections of the major pathologies found in the *K243R/+* mice. The insets show high-magnification images. (C) H&E staining of spleens. (D–F) Analysis of lymph node cells. (D) Freshly isolated lymph node cells were immunostained using the indicated antibodies and subjected to flow cytometric analysis. (E) Lymph node sections from the *K243R/+* mice were stained using an anti-B220 antibody and were counterstained with hematoxylin. (F) Wright-Giemsa staining of cytocentrifuged lymph node cells. (G) Megakaryocytic leukemia in the *K243R/+* mice. The spleens were stained with H&E (left) or anti–von Willebrand factor (vWF) antibody and hematoxylin (right).

and size comparable to WT, and four of them were able to grow in culture with growth retardation (Fig. 1 F). In comparison, four blastocysts stopped proliferating from E6.5: these embryos were obtained at a frequency similar to that of homozygous mutant *BubR1*$^{K243R/K243R}$.

We were unable to obtain DNA that was adequate for genotyping the presumed homozygous mutant embryos. Therefore, as an alternative approach, 17 E6.5 embryos, which were derived from three intercrosses of *K243R/+* parents, were fixed and embedded in paraffin and apoptosis was examined. Four out of seventeen embryos exhibited an abnormal morphology with massive TUNEL staining (Fig. 1 G). These phenotypes and apoptosis were observed only in *K243R/+* intercrosses and were not observed when the *K243R/+* mice were mated with WT mice. Therefore, these data suggest that *BubR1*$^{K243R/K243R}$ embryos die as a result of apoptosis at approximately E6.5.

Robust cancer development in *K243R/+* mice

Progeny of the *K243R/+* intercrosses, WT mice (n = 41) and *K243R/+* mice (n = 121) on a mixed 129 × C57BL/6 background, were monitored until 38 mo of age. Although no overt developmental defects were noted, a significant incidence of spontaneous tumor development was observed between 60 and 70 wk after birth in the *K243R/+* mice (Fig. 2 A). A marked increase in malignant tumor development (23.1%, n = 28) was observed (Table 1 and Fig. 2 A, right) for both solid (10.7%, n = 13) and hematologic (12.4%, n = 15) tumors. The tumors were found in a variety of tissues (Fig. 2 B), with an overall tumor incidence of 38% (Table 1 and Fig. 2 A, left).

Splenomegaly was frequently observed when the *K243R/+* mice were killed at ∼60 wk after birth (Fig. 2 C, right). These splenomegalies included B cell lymphomas, which exhibited white pulp expansion with B220 positivity in either a follicular or diffuse pattern. The level of B220 varied, and a distinction between the B and the presumed T cell area was not observed among the B cell lymphomas examined (9.1%, n = 11; Fig. 2, B and C). In the lymph nodes, B cell hyperproliferation was observed (Fig. 2 D) and consisted of large, often fragmented, nuclei with irregular shapes (Fig. 2, E and F). Notably, in two cases, we observed the invasion of B cells into the liver (Fig. 2 B, bottom) and into the lung (not depicted). In one of these samples, nodules measuring 0.7 cm in diameter were detected in the mesenteric lymph nodes, which were populated with leukemic B and activated T cells. In addition, several of the lymphomas developed into B cell leukemias (2.5%, n = 3). In the other

Published July 22, 2013

Table 1. **Tumor spectrum and analysis**

Tumor types	*BubR1*$^{K243R/+}$ (*n* = 121)	*BubR1*$^{+/+}$ (*n* = 41)
Malignant tumors	28 (23.1%)	2 (4.8%)
Malignant solid tumors	13 (10.7%)	1 (2.4%)
Hepatocellular carcinoma	6 (5.0%)	
Sarcoma[a]	4 (3.3%)	1 (2.4%)
Adenocarcinoma[b]	2 (1.7%)	
Other cancer[c]	1 (0.8%)	
Hematologic malignancies	15 (12.4%)	1(2.4%)
Megakaryocyte leukemia	1 (0.8%)	
B cell lymphoma	11 (9.1%)	1 (2.4%)
Metastatic lymphoma/leukemia	3 (2.5%)	
Benign tumors[d]	18 (14.9%)	
Total tumor incidence	46 (38.0%)	2 (4.8%)

[a]Sarcomas included smooth muscle sarcoma (*n* = 2), endometrial stromal sarcoma (*n* = 1), and angiosarcoma (*n* = 1) in *K243R/+* mice. A single fibrosarcoma was found in the WT.
[b]Adenocarcinomas included lung adenocarcinoma (*n* = 1) and rectal adenocarcinoma (*n* = 1) in *K243R/+*.
[c]Other cancer included skin cancer.
[d]Benign tumors included simple cysts in the genital tract (*n* = 10), hemangioma (*n* = 5), epidermal cyst (*n* = 1), acrochordon (*n* = 1), and mesenchymal fibroma (*n* = 1).

sample, large granular cells populated the spleen, which displayed von Willebrand factor positivity (Fig. 2 G), suggestive of megakaryocytic leukemia (0.8%, *n* = 1; Hao et al., 2006).

Aneuploidy and premature sister chromatid separations (PMSCS) in *K243R/+* mouse embryonic fibroblasts (MEFs)

Analysis of metaphase chromosome spreads revealed near-diploid-type aneuploidy in the *K243R/+* MEFs. In fact, 67% of the cells exhibited aneuploidy with chromosome loss or gain. In comparison, the rate of polyploidy was comparable to that of WT MEFs (Fig. 3 A). PMSCS (Fig. 3 B, right) was increased 5.5-fold in *K243R/+* MEFs compared with controls (Fig. 3 C). PMSCS result from a compromised SAC (Michel et al., 2001) or from the failure to maintain the centromeric cohesion that is mediated by Shugosin and phosphatase PP2A (Tang et al., 2006; Rivera and Losada, 2009). Addition of MG132 to cells before preparing the chromosome spreads restored the incidence of PMSCS in the *K243R/+* MEFs to a level comparable to that of the WT control (Fig. 3 C). Because MG132 treatment preferentially interferes with the destruction of securin and cyclin B, these data suggest that the PMSCS caused by the partial loss of BubR1 acetylation is a response to premature activation of APC/C.

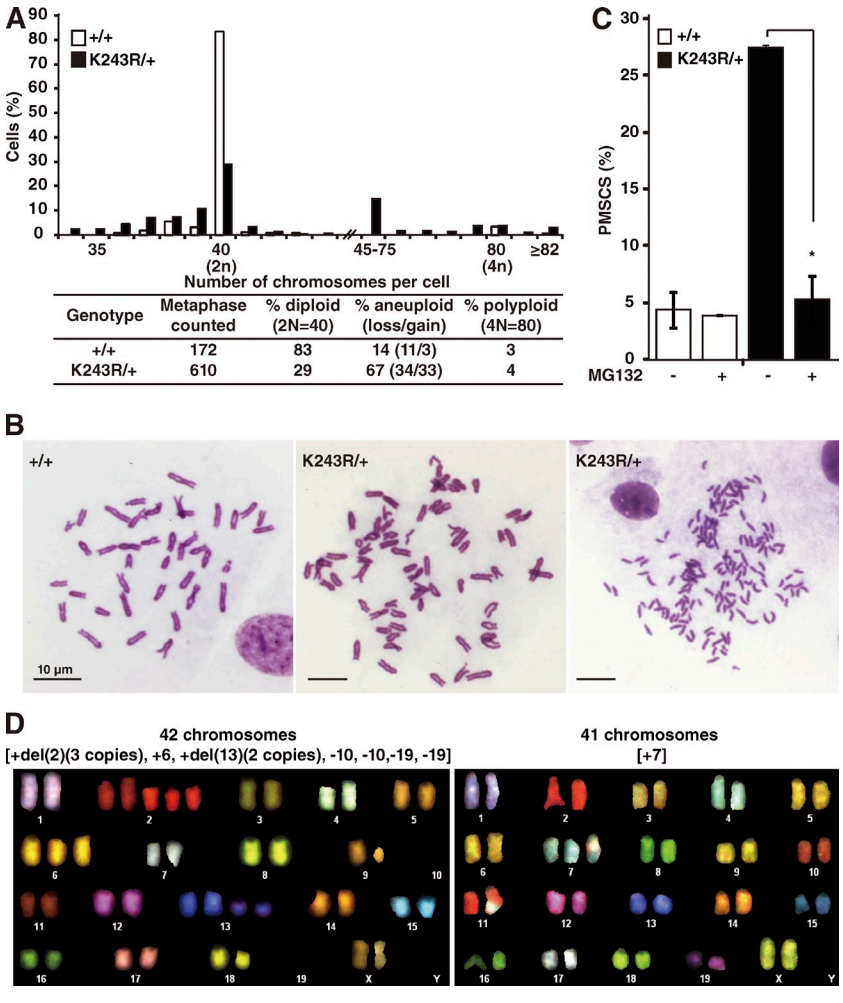

Figure 3. ***K243R/+* MEFs exhibit aneuploidy with a high incidence of PMSCS.** (A) The percentage of cells displaying the indicated number of chromosomes. The results are from three and five different WT and *K243R/+* MEFs, respectively. (bottom) The table summarizes the analysis of the chromosome numbers in the histogram. (B) Representative images of the metaphase chromosome spreads. (C) Incidence of PMSCS. MEFs were treated with MG132 for 2 h or left untreated, and chromosome spreads were analyzed (WT, *n* = 96; WT treated with MG132, *n* = 51; *K243R/+*, *n* = 91; *K243R/+* treated with MG132, *n* = 70; *, P = 0.04). Cells containing more than one chromosome featuring PMSCS were scored. (D) Two examples of SKY analysis of the *K243R/+* MEFs cultured for 27 passages are shown.

Published July 22, 2013

Table 2. **SKY analysis in *K243R/+* MEFs at passage 27**

Metaphases	Karyotypes
1	42 [XX, +del(2) (three copies), +6, +del(13) (two copies), −10, −10, −19, −19]
2	41 [XX, +7]
3	40 [X, −X, t (4:X)]
4	42 [XX, +17, +17]
5	42 [XX, +9, +18]
6	41 [XX, +2]
7	40 [XXX, +5, −17, −17]
8	39 [−X, −X, +del(10), +8]
9	41 [XX, +3]
10	40 [XX]
11	40 [XX]
12	40 [XX]
13	40 [XX]
14	40 [XX]

The karyotypes of 14 metaphases are presented. del, deletion; t, translocation.

Next, chromosomes from *K243R/+* MEFs at a late passage were subjected to spectral karyotyping (SKY). Aneuploidy was significant, and chromosome translocations were also detected in one case out of 14 (Fig. 3 D and Table 2). Signs of chromosome pulverization, like those from errors in mitosis (Crasta et al., 2012), were also detected (Fig. 3 D, left, chromosomes 2 and 13). As shown in the representative data, the cells exhibited heterogeneity in chromosome instability until MEFs reached passage 27 (Table 2). Aneuploidy was detected consistently in lymphoma/leukemia cells. Indeed, >50% of the splenic cells and lymphomas exhibited aneuploidy, and PMSCS were apparent in tumors as well (Table 3).

Weakened SAC and chromosome missegregation in *K243R/+* MEFs

Next, we assessed the integrity of the SAC. First, the mitotic index was measured after challenge with a MT polymerization inhibitor nocodazole (Noc) or the depolymerization inhibitor paclitaxel (Taxol). The MEFs in culture were treated with Noc or Taxol, and cell aliquots collected at the indicated times were subjected to immunostaining using MPM-2 (mitotic monoclonal 2) and propidium iodide staining. The mitotic cells that were positive for MPM-2 staining with 4C DNA content were analyzed by flow cytometry (Choi et al., 2009). This analysis demonstrated that the *K243R/+* MEFs exhibited a weakened SAC (Fig. 4 A).

We assessed the localization of Mad2 at the unattached KTs in untreated prometaphase and Noc- or Taxol-treated WT, *K243R/+*, and haploinsufficient *BubR1* MEFs (*BubR1*$^{+/-}$; Wang et al., 2004). The number of Mad2 foci at the KTs was highest when MTs were completely depolymerized after treatment with 3.3 μM Noc. Slightly lower but similar levels of Mad2 were detected at KTs in untreated prometaphase cells. Upon Taxol treatment, the number of Mad2 at KTs decreased to ∼1/3 of that in Noc-treated cells (Fig. 4 B). Nevertheless, the pattern and extent of Mad2 localization at KTs were similar between WT, *K243R/+*, and haploinsufficient *BubR1* cells. Similar results were obtained with Mad1 (Fig. 4 B). According to the Mad2 template model, the presence of the Mad1/Mad 2 complex at unattached KTs predicts the cytosolic propagation of the SAC signal (De Antoni et al., 2005). Therefore, these results suggest that the establishment of the initial SAC signal is intact in *K243R/+* cells.

We then analyzed the formation of MCC. In Noc-treated MEFs, BubR1 levels were lower in *K243R/+* cell lysates, confirming that nonacetylated BubR1 is unstable during mitosis because this protein is a substrate of APC/C. When proteolysis was inhibited (Fig. 4 C, +Noc+MG132), BubR1 levels were restored in the lysates. Immunoprecipitation (IP) of BubR1 immune complex demonstrated that Cdc20, Bub3, and Mad2 levels were decreased in *K243R/+* cells compared with WT cells, even though similar amounts of BubR1 were immunoprecipitated in Noc-treated condition (Fig. 4 C, +Noc). Similarly, Cdc20, Bub3 and Mad2 in immunoprecipitated BubR1 complexes from *K243R/+* cells were restored to levels comparable to those from complexes from WT cells when proteolysis was inhibited (Fig. 4 C, +Noc+MG132). As the ratio of WT BubR1 to K243R was 1:1 in *K243R/+* MEFs (Fig. 4 D), these results suggest that acetylation-deficient BubR1 (K243R) is capable of binding to the other MCC components and to APC. However, the degradation of K243R (Choi et al., 2009) in prometaphase (Noc-treated condition) results in a failure to maintain MCC.

The amount of BubR1 at the KTs was assessed in chromosome spreads after Noc treatment. The result showed that the level of BubR1 at KT was lowest in *BubR1*$^{+/-}$ cells with higher levels in *K243R/+* cells and the highest in WT cells (Fig. 4 E). As the antibody used in this assay recognizes both WT BubR1 and K243R, this result indicates that K243R localizes to KT and is degraded during mitosis (Fig. 4 E).

Next, we measured the mitotic timing in *K243R/+* cells. *K243R/+* mice were crossed with *GFP-H2B* transgenic mice.

Table 3. **Chromosome analysis of lymphoma/leukemia derived from *K243R/+* mice**

Genotype	Tissue/tumor	Age (n)	Metaphase counted	Diploid (2N = 40)	Aneuploid (loss/gain)	PMSCS
		wk		%	%	%
BubR1$^{+/+a}$	Spleen	60 (3)	65	95.5	4.5 (2.25/2.25)	0
BubR1$^{K243R/+a}$	Spleen	60 (6)	319	48	52 (42/10)	5
BubR1$^{K243R/+}$	Lymphoma	57	98	46	54 (33/19)	31
BubR1$^{K243R/+}$	Lymphoma/leukemia 1	65	76	62	38 (22/16)	14
BubR1$^{K243R/+}$	Lymphoma/leukemia 2	104	137	51	49 (30/19)	19

[a]Normal splenocytes from adult mice of the indicated genotypes and ages. Splenocytes were activated using 10 μg/ml lipopolysaccharides, and a chromosome spread was performed.

Published July 22, 2013

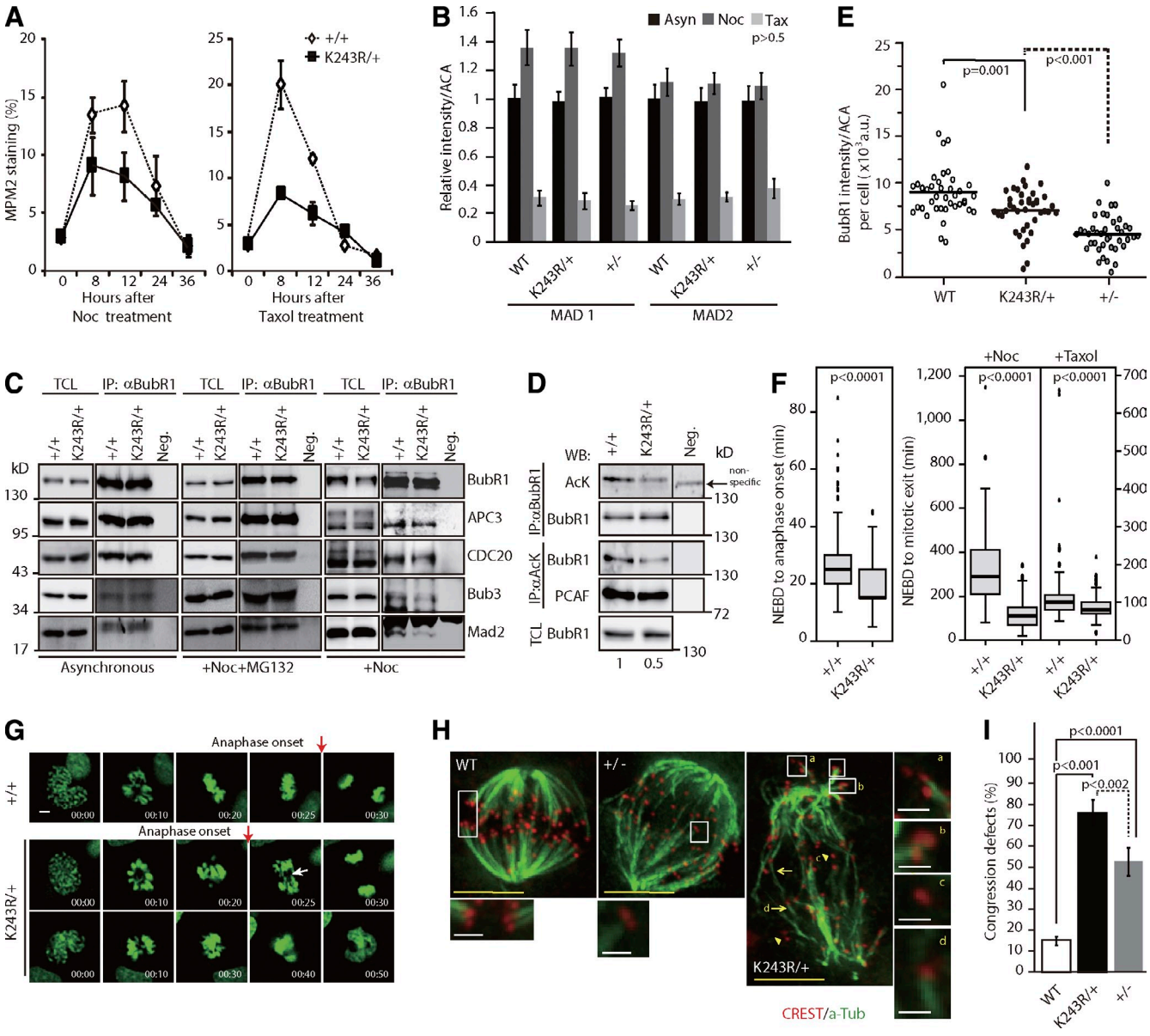

Figure 4. **Weakened SAC and congression failure in *K243R/+* MEFs.** (A) WT and *K243R/+* MEFs were treated with 200 ng/ml nocodazole (Noc; left) or 2 µM paclitaxel (Taxol; right). The cells were collected at the indicated time points, stained with MPM-2 and 7-amino-actinomycid D, and analyzed by flow cytometry. The results and SDs are from three independent experiments. (B) WT, *K243R/+*, and *BubR1*$^{+/-}$ MEFs were treated with 3.3 µM Noc or 2 µM Taxol or left untreated. Cells were subjected to coimmunostaining with anti-Mad2 or -Mad1 antibody and FITC-conjugated anti–α-tubulin antibodies. Mad2 or Mad1 at the KTs with similar intensities were scored in each setting (Asyn; prometaphase cell in untreated sample). 10 unaligned/unattached KTs were analyzed per cell. The result is from three independent experiments of 35 different cells each. Relative value compared with the untreated prometaphase cell (Asyn) in WT is depicted by bar graphs (mean ± SEM; $n > 350$ KTs each). (C) The asynchronous and mitotic MEFs of WT and *K243R/+*, respectively, were subjected to IP and WB as indicated. For the mitotic extracts, the cells were serum starved for 26 h, released for 20 h, and treated with nocodazole for 7 h. In Noc + MG132-treated MEFs, Noc treatment was followed by MG132 treatment for 2 h before lysis. IP with anti-HA antibody was included as a negative control (Neg.). A sample representing 3% of the total cell lysate (TCL) was loaded as a control. (D) Assessment of BubR1 acetylation levels in WT and *K243R/+* MEFs. The MEFs were treated with Noc and MG132 as in C and subjected to IP and WB as indicated. A sample representing 1% of the TCL was loaded as a control. The ratio of AcK243/total BubR1, when the level in +/+ cells is normalized to 1, was the same for both the anti-BubR1 and anti-AcK IPs and is marked below each lane. IP with a mixture of rabbit serum and 12CA5 anti-HA antibody is shown as a negative control for each panel (Neg.). Only a non-specific band migrating just below the band recognized by anti-AcK antibody (top left two lanes) was detected. Black lines in the top four panels indicate the removal of an intervening lane for presentation purposes. (E) Quantification of BubR1 at KTs in chromosome spreads after treatment with 200 ng/ml Noc. The level of BubR1, determined by anti-BubR1 immunofluorescence in Noc-treated prometaphase MEFs, was scored in WT, *BubR1*$^{+/-}$, and *K243R/+* MEFs. Each dot represents the mean BubR1 intensity calculated from 20 randomly picked KTs per cell. 40 chromosome spreads from each genotype were scored in two independent experiments. Mean value is indicated with a line (mean ± SEM; $n > 800$ KTs each). (F) Statistical mitotic timing from the NEBD to anaphase onset. The MEFs were subjected to time-lapse microscopy with or without treatment with 200 ng/ml Noc or 2 µM Taxol. Images were captured every 5 min, and the live images were processed for 36 h. Without a spindle poison, mitosis required an average of 25 min in the WT cells ($n = 170$) and ~20 min in the *K243R/+* MEFs ($n = 153$). After spindle poison exposure, the WT cells remained in mitosis for 331 min with Noc ($n = 66$) and 106 min with Taxol ($n = 218$). The *K243R/+* MEFs exited mitosis (chromosome decondensation) within 117 min with Noc treatment ($n = 144$) and within 87 min with Taxol treatment ($n = 191$). The bars in the box represent the median values. The outliers (open circles) and suspected outliers (asterisks), as determined by statistical analysis, are marked. (G) Representative images captured at the indicated time points from NEBD without

Published July 22, 2013

MEFs from WT mice expressing *GFP-H2B (+/+*; *GFP-H2B*) and from *K243R/+* mice expressing *GFP-H2B* (*K243R/+*; *GFP-H2B*) were subjected to time-lapse microscopy to measure the mitotic timing from nuclear envelope breakdown (NEBD) to the onset of anaphase. Mitotic timing was ∼5 min shorter in the *K243R/+* MEFs (Fig. 4 F, left) than in the WT MEFs. In the presence of either Noc or Taxol, the duration of mitotic arrest was greatly reduced in the *K243R/+* MEFs (Fig. 4 F, right); however, the effect on mitotic timing in response to Noc was more profound than to Taxol.

In the captured live-cell imaging, chromosome missegregation was apparent in the *K243R/+* MEFs, compared to WT (Fig. 4 G, first row; and Video 1), even in the absence of spindle poisons. Indeed, 85% of the *K243R/+* MEFs exhibited chromosome segregation without forming a distinct metaphase plate, yielding lagging chromosomes and chromosome bridges (Fig. 4 G, second row; and Video 2), and 15% of *K243R/+* MEFs exited mitosis without proper chromosome alignment (Fig. 4 G, third row; and Video 3). This result indicates that *K243R/+* MEFs have problems in chromosome alignment.

The absence of BubR1 results in failure to maintain stable KT–MT attachments (Lampson and Kapoor, 2005), and one study suggested that the BubR1 N terminus is required for the KT–MT interaction in metaphase (Malureanu et al., 2009). To assess whether BubR1 acetylation is involved in the stable attachments of K-fibers to the chromosomes at metaphase, a cold-stable MT assay (Rieder, 1981) was performed. As MG132 treatment was included in the assay, it blocks the degradation of K243R. Therefore, both K243R and WT BubR1 are present in *K243R/+* MEFs. The *K243R/+* MEFs exhibited severe defects in KT–MT attachment (Fig. 4 H, *K243R/+*). Interestingly, defects in congression were more profound in *K243R/+* than in *BubR1*$^{+/-}$ (Fig. 4 I). Thus, these results confirm that acetylation of BubR1 is required for chromosome congression.

Acetylation of BubR1 is required for recruiting PP2A-B56α phosphatase to KT

We assessed whether binding of BubR1 to CENP-E or Blinkin (KNL1) was affected by the acetylation status. BubR1 associates with CENP-E (Chan et al., 1999; Abrieu et al., 2000; Mao et al., 2003; Weaver et al., 2003), which is the kinesin-7 motor protein at KT that enables the monotelic polar chromosomes to glide along the existing K-fiber toward the cell center (Kapoor et al., 2006) to aid chromosome congression (Kim et al., 2010). BubR1 also binds to KNL1/Blinkin (Kiyomitsu et al., 2007; Bolanos-Garcia et al., 2011), which is a constituent of the KMN network that provides the MT-binding interface in the KT required for the KT–MT interaction.

For this study, we took advantage of the stable inducible HeLa cell lines in which a single copy of FLAG-tagged *WT-BubR1*, *K250R* (acetylation deficient), or *K250Q* (acetylation mimetic) is integrated into the genome at a flippase recognition target (FRT) site. The endogenous BubR1 was depleted in these cells using siRNA transfection, and the expression of the ectopic *BubR1*, *K250R*, or *K250Q* was induced. After IP and Western blot (WB) of cell lysates, we found that the acetylation status of BubR1 affected CENP-E binding. The K250Q protein binding to CENP-E was increased ∼1.2-fold, whereas binding of the K250R to CENP-E was decreased ∼0.7-fold (Fig. 5 A, right). Meanwhile, KNL1/Blinkin binding was unaltered (Fig. 5 A).

CENP-E assembly at the KT requires BubR1 (Johnson et al., 2004). Therefore, we determined whether BubR1 acetylation deficiency affected CENP-E localization. WT, *K243R/+*, and *BubR1*$^{+/-}$ MEFs were subjected to the cold MT assay combined with immunofluorescence with an anti–CENP-E antibody (Fig. 5 B). The KT–MT attachment was severely impaired in the *K243R/+* cells (Fig. 5 B). The CENP-E to BubR1 ratio at the KT was similar in the WT and the *BubR1*$^{+/-}$ cells, although BubR1 and CENP-E at the KT was lower in the *BubR1*$^{+/-}$ MEFs (Fig. 5, B and C, right). In comparison, the level of CENP-E at KT was reduced to ∼50% of the WT level in *K243R/+* cells (Fig. 5, B and C, right), although the total BubR1 level was comparable to that in WT cells as a result of the treatment with MG132 (Fig. 5 C, left). As the total level of CENP-E in *K243R/+* MEFs was unaltered (Fig. 5 D), the observed decrease of CENP-E at KTs in *K243R/+* MEFs suggests that binding to BubR1 is required for CENP-E localization at KTs.

Upon depletion of CENP-E in HeLa cells, most of the chromosomes align at the metaphase plate with some near the poles (Lampson and Kapoor, 2005). In comparison, the congression failure induced by the BubR1 acetylation deficiency was much more severe. Overexpression of *CENP-E-GFP* in *K243R/+* MEFs did not rescue the congression defects (Fig. 5 E, CENP-E), whereas ectopic expression of the human form of acetylation-mimetic *BubR1* (*K250Q*) rescued the KT–MT attachment in *K243R/+* MEFs (Fig. 5 E, K250Q) and in BubR1-depleted HeLa cells (Fig. S2 A, K250Q). These results suggest that the lowered binding of acetylation-deficient BubR1 to CENP-E does not fully explain the congression failure in *K243R/+*.

MTs are bound to the KT through the conserved KMN network (Cheeseman et al., 2006). In this network, the Ndc80 (Hec1 in human) complex is the primary contact point for KT–MT attachment (DeLuca et al., 2006; Wei et al., 2007; Sundin and Deluca, 2010). During the error correction process of mitosis, Aurora B phosphorylates Ndc80 and other KMN proteins in sequence (Welburn et al., 2010), resulting

Noc treatment. Of the 20 *K243R/+* MEFs, 17 displayed congression failure (second row; Video 2) and 3 exited mitosis without segregation (third row; Video 3). See Video 1 for the WT MEF control (first row). The timing of the onset of anaphase is marked. The white arrow indicates the lagging chromosome. NEBD: 00:00. Bar, 5 µm. (H) WT, *BubR1*$^{+/-}$, and *K243R/+* MEFs were treated with MG132 for 2 h and subjected to cold MT assay, followed by staining with anti–α-tubulin and CREST. Enlarged images of the insets show the properly attached MT in WT cells; syntelic attachment in *BubR1*$^{+/-}$ cells; and unattached (c), syntelic (a and b), and monotelic attachment (d) in *K243R/+* cells. Green, α-tubulin; red, CREST immunostaining. Bars: (yellow) 5 µm; (white) 1 µm. (I) The congression defects were scored in cells from each mouse strain in the absence of MT poison, and data are shown as bar graphs (mean ± SEM). Number of cells scored: WT, *n* = 75; *K243R/+*, *n* = 102; *BubR1*$^{+/-}$, *n* = 60.

Published July 22, 2013

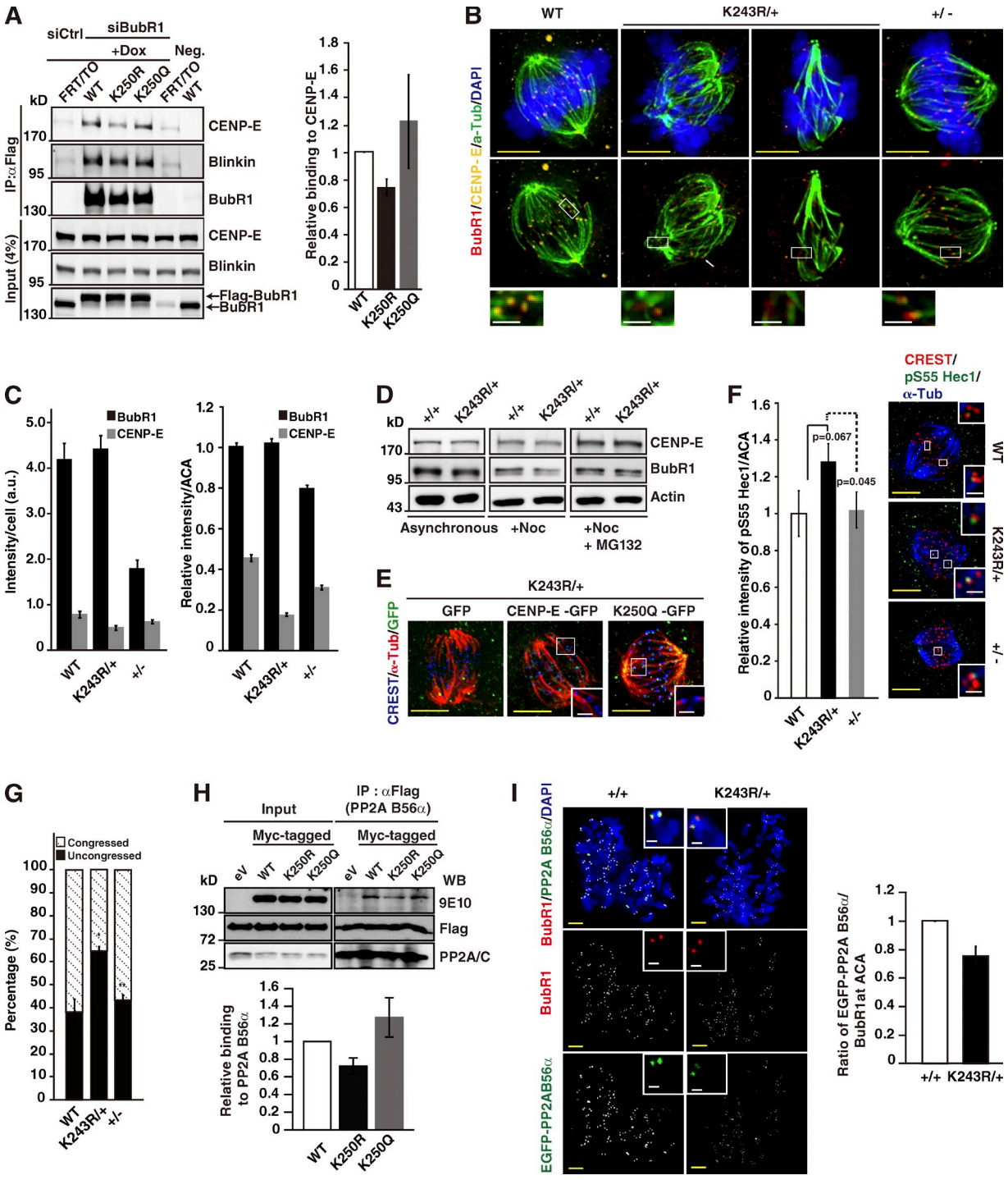

Figure 5. **How BubR1 acetylation is involved in KT–MT interaction.** (A) The HeLa-FRT-BubR1, -K250R, or -K250Q cells were depleted of endogenous *BubR1*, and the expression of the indicated FLAG-tagged *BubR1* constructs was induced by doxycycline treatment. The cells were synchronized in mitosis using the thymidine block and treated with nocodazole/MG132. BubR1 complexes were immunopurified using an anti-FLAG (M2) antibody, followed by WB using the indicated antibodies. The total lysates were included in the WB as an input control. Immunoprecipitated CENP-E bands were normalized to BubR1, and the binding affinities of each BubR1 to CENP-E were determined. The relative binding to CENP-E and the SDs in the graph are from four independent experiments (right). (B) Immunostaining of CENP-E and CREST in WT, *K243R/+*, and *BubR1*$^{+/-}$ MEFs after the cold MT assay. The cells were treated with MG132 before fixation. Enlarged images are shown at the bottom. Red, BubR1; yellow, CENP-E; green, α-tubulin. Bars: (yellow) 5 µm; (white) 1 µm. (C) Relative levels of BubR1 and CENP-E from B, in the presence of MG132, as measured by fluorescence intensities at the cellular level (left) and at KTs (right) are represented by bar graphs. Fifty cells in each genotype were scored in two independent experiments (mean ± SEM; $n > 500$ KTs). (D) WB analysis of CENP-E and BubR1 from lysates prepared from untreated, Noc-treated, or Noc + MG132-treated MEFs. The blot was reprobed with anti-actin antibody as a loading control. (E) GFP-tagged *CENP-E* expression construct (Kim et al., 2010) or *K250Q* expression construct was transfected into *K243R/+* MEFs. 1 d after transfection, MEFs were synchronized via serum starvation and released into mitosis with change with fresh media supplemented with 16% FBS. 24 h later, cells were treated with MG132 for 2 h and subjected to cold MT assay. Representative images are shown. Ectopic expression of *CENP-E-GFP* or *K250Q-EGFP* was detected by green fluorescence. *EGFP*-expressing construct was transfected for control. Enlarged images of the insets (excluding GFP) are shown at the right. Red, α-tubulin; blue, CREST staining; green, GFP. Bars: (white) 1 µm; (yellow) 5 µm. (F) Comparison

Published July 22, 2013

in the disassembly of incorrectly attached MTs (Lampson and Cheeseman, 2011). As the chromosomes biorient, excess Aurora B activity is counteracted and Ndc80 is dephosphorylated, establishing the stable KT–MT attachment before chromosome segregation.

As the number of K-fiber was reduced in *K243R/+* cells (and K250R-expressing cells), we determined the phosphorylation of Hec1 (human Ndc80) at the KT using phospho-S55–specific Hec1 antibody (anti-pHec1; DeLuca et al., 2011). After 2 h in MG132, MEFs were subjected to cold MT assays and immunofluorescence with anti-pHec1 antibody (Fig. 5 F, right). *K243R/+* MEFs displayed a 1.3-fold higher level of pHec1 than either WT or *BubR1*$^{+/-}$ cells (Fig. 5 F, left). When assessed for the error correction capability from the treatment of Monastrol (Lampson et al., 2004), *K243R/+* MEFs displayed a markedly higher percentage of uncongressed chromosomes compared with WT or *BubR1*$^{+/-}$ MEFs (Fig. 5 G).

Recently, BubR1 was found to bind to B56α subunit of PP2A phosphatase after phosphorylation. BubR1 binding to PP2A-B56α recruits PP2A phosphatase activity to KTs and counteracts Aurora B activity on KMN (Suijkerbuijk et al., 2012; Kruse et al., 2013). As the hyperphosphorylation of Hec1 in *K243R/+* cells indicated excessive Aurora B activity, we assessed the binding properties of acetylation-deficient BubR1 to PP2A-B56α. Myc-tagged *WT-BubR1*, *K250R*, or *K250Q* were ectopically expressed in HeLa-FRT cells that stably express *PP2A-B56α* (Kruse et al., 2013). In IP and WB, we found that binding to PP2A-B56α was reduced to ∼75% by the BubR1 acetylation deficiency (Fig. 5 H). Immunofluorescence analysis in Noc-treated chromosome spreads confirmed that PP2A-B56α binding to BubR1 and recruitment to KTs were reduced to ∼75% in *K243R/+* MEFs (Fig. 5 I and Fig. S2 B). Immunostaining of Noc and MG132–treated cells with an antibody that recognizes the phosphorylation of BubR1 at T680 (p680), the site phosphorylated by Plk1 that is involved in the recruitment of PP2A-B56α (Suijkerbuijk et al., 2012), revealed that *K243R/+* prometaphase cells exhibited lower p680 at KTs (Fig. S2 C); however, the level of p680 correlated with the level of BubR1 at KTs. Collectively, BubR1 acetylation is involved in the recruitment of PP2A-B56α to KTs for chromosome congression.

Micronuclei in MEFs, regenerating hepatocytes, and hepatocellular carcinoma

Failure in bipolar spindle attachment activates SAC, arresting the cells in mitosis. Delay in mitosis was observed in cells expressing BubR1 mutants that are defective in binding to PP2A-B56α (Kruse et al., 2013). In comparison, *K243R/+* cells display shortened mitotic timing. Because of the weakened SAC despite the failure in chromosome–spindle attachment, *K243R/+* cells exhibited marked increase of micronuclei, which result from lagging chromosomes (Fig. 6, A and B). The incidence of micronuclei was found to be ∼18% in *K243R/+* MEFs (Fig. 6 B). An interesting paper showed that micronuclei do not degenerate but persist through several cell divisions (Crasta et al., 2012). It showed that because micronuclei are uncoupled with DNA replication and repair, micronuclei contain damaged DNA and pulverized chromosomes (Crasta et al., 2012).

Assessment of the DNA damage in the micronuclei revealed γ-H2AX positivity (Fig. 6 C, left). Notably, general DNA damage was not altered in *K243R/+* cells (Fig. 6 C, right). The micronuclei were consistently found in the regenerating hepatocytes after hepatectomy (Mitchell and Willenbring, 2008) with a marked increase in *K243R/+* mouse livers (Fig. 6 D). Paraffin sections of hepatocellular carcinoma from *K243R/+* mice also contained micronuclei and lagging chromosomes (Fig. 6 E). Combined with the observation that SKY revealed signs of chromosome pulverization (Fig. 3 D), the persistence of micronuclei from primary cells to cancer suggests an interesting possibility that the micronuclei facilitated DNA breakage and chromosome pulverization that contributed to tumorigenesis in *K243R/+* mice.

The inefficient DNA repair in the micronuclei indicates that they could be the source of genetic alterations. In this line of thinking, it is interesting that 8 out of 11 tumors possessed mutant *p53*: the mutations were predominantly missense mutations, small deletions, and insertions (Table 4). Using the International Agency for Research on Cancer TP53 database, we determined that several of the mutations affected p53 function (e.g., impaired transcriptional or DNA-binding activities) and were correlated to mutations found in human cancers (Table 4). Collectively, these findings suggest that *K243R/+* cells are susceptible to acquisition of additional mutations.

of phosphorylated Hec1 in metaphase cells. MEFs from WT, *K243R/+*, and *BubR1*$^{+/-}$ mice were treated with 10 µM MG132 for 2 h and subjected to cold MT assay. The levels of pHec1 scored in two independent experiments are shown in bar graphs (mean ± SEM; $n > 450$ KTs; number of cells scored: WT, $n = 23$; *K243R/+*, $n = 34$; *BubR1*$^{+/-}$, $n = 25$). Representative images are shown at the right with enlarged images of individual KTs in the insets. Bars: (white) 1 µm; (yellow) 5 µm. (G) MEFs were treated with Monastrol for 3 h, washed extensively, and released 1 h in the presence of MG132 and subjected to cold MT assay. Congressed and uncongressed chromosomes were scored in two independent experiments and presented in the bar graphs (mean ± SEM; number of cells scored: WT, $n = 71$; *K243R/+*, $n = 78$; *BubR1*$^{+/-}$, $n = 73$). Asterisks mark significant p-values when compared with WT (*, P = 0.1; **, P = 0.5). (H) Myc-tagged *WT-BubR1*, *K250R*, or *K250Q* expression constructs were transfected into *PP2A-B56α*–expressing HeLa-FRT cells (Kruse et al., 2013). Expression of *PP2A-B56α* was induced with doxycycline followed by cell synchronization and mitotic arrest with the treatment of Noc and MG132 to inhibit proteolysis. The cells were subjected to IP and WB. WB of the catalytic subunit of PP2A (PP2A/C) was included for normalization of IP (top). Relative binding affinity to PP2A-B56α was calculated by measuring 9E10 band intensities (WT, K250R, and K250Q, respectively) in FLAG immune complex (PP2A-B56α). SDs in bar graphs are from four independent experiments (bottom). eV, empty vector. (I) *EGFP-PP2A-B56α*–expressing construct was transfected into *K243R/+* MEFs. 24 h later, MEFs were treated with 200 ng/ml Noc for 4 h, and then subjected to chromosome spread and immunofluorescence assay. BubR1 was detected by immunofluorescence and PP2A-B56α by the fluorescence of GFP (left). This experiment was done in the absence of MG132. Fluorescence intensity of PP2A-B56α relative to BubR1 at KT was scored in WT and *K243R/+* cells and depicted as a histogram (right). The results are from two independent experiments of >600 KTs (mean ± SEM; number of cells: WT, $n = 33$; *K243R/+*, $n = 32$; P = 0.061). Red, BubR1; green, PP2A-B56α; blue, DAPI. Bars: (white) 1 µm; (yellow) 5 µm.

Published July 22, 2013

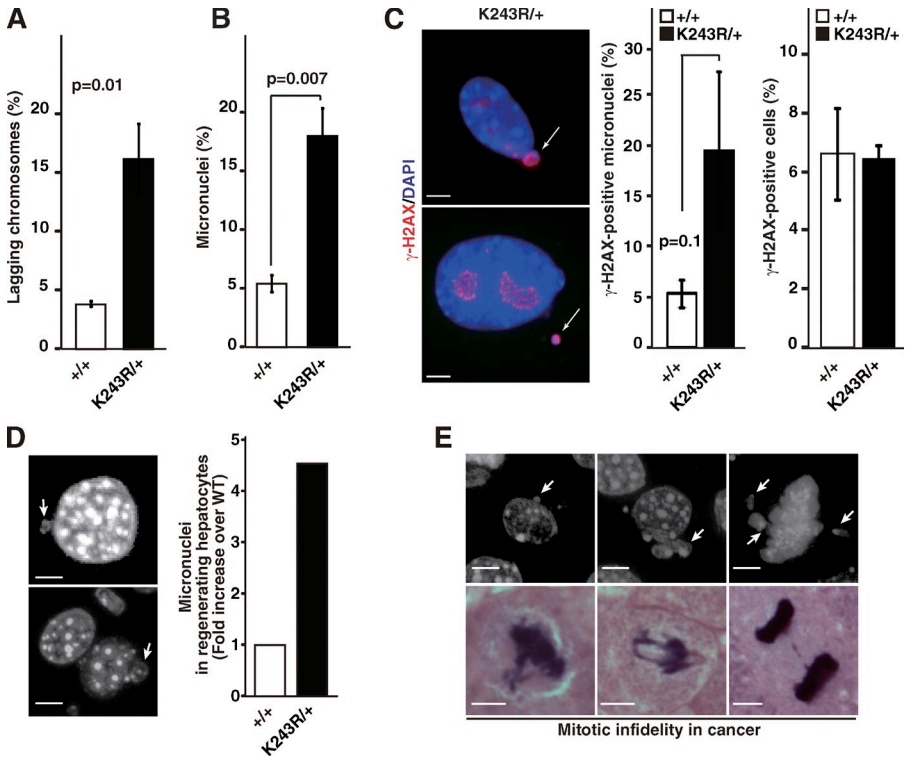

Figure 6. **Marked increase of micronuclei in *K243R/+* mice.** (A) The frequency of MEFs that display lagging chromosomes (WT, *n* = 52; *K243R/+*, *n* = 153). (B) The frequency of micronuclei shown in bar graphs (WT, *n* = 52; *K243R/+*, *n* = 1,976). (C) γ-H2AX–positive micronuclei (arrows) in *K243R/+* MEFs. The cells were stained with a γ-H2AX antibody, and DNA was counterstained with DAPI. (left) The incidence of γ-H2AX–positive micronuclei (WT, *n* = 1,463; *K243R/+*, *n* = 1,132). (right) Cellular DNA damage in WT and *K243R/+* MEFs (WT, *n* = 1,463; *K243R/+*, *n* = 1,132). The results in A–C are from two independent experiments (mean ± SEM). (D) Paraffin-embedded sections of livers from WT or *K243R/+* mice after partial hepatectomy were stained with H&E. Three animals each were subjected to partial hepatectomy. Micronuclei in regenerating hepatocytes (arrows) are compared as fold increase on the right: WT, 0.4% (3 out of 693 cells); *K243R/+*, 2.0% (21 out of 1,069). (E) Micronuclei or nuclear blebs (top, arrows) and lagging chromosomes (bottom) observed in the paraffin-embedded sections of hepatocellular carcinoma from the *K243R/+* mice. Bars, 10 µm.

Discussion

BubR1 haploinsufficiency in mice (*BubR1*$^{+/-}$) resulted in abnormal megakaryopoiesis, but spontaneous cancer development was not observed (Wang et al., 2004). Unexpectedly, BubR1 insufficiency in hypomorphic mice (*BubR1*^{H} allele) exhibited a premature aging phenotype (Baker et al., 2004). In comparison, in *K243R/+* mice, premature aging was not observed and, strikingly, a high incidence of spontaneous tumorigenesis, both solid and hematologic malignancies, was observed (Table 1). These differences suggest that the effects of a BubR1 acetylation deficiency are not simply because of a decrease in protein level. Indeed, in assays for chromosome congression, *K243R/+* MEFs displayed significant defects in the KT–MT interaction, and these defects were even worse than those observed in the haploinsufficient *BubR1* MEFs. As *BubR1*$^{+/-}$ and hypomorphic *BubR1* MEFs also exhibit aneuploidy, whole chromosome aneuploidy alone cannot be the cause of spontaneous tumorigenesis.

In dividing cells, chromosome movement is coupled with MT dynamics and attachment. Aurora B kinase is essential in correcting the improperly attached chromosomes (Lampson et al., 2004) via phosphorylation of the contact point of the MTs at the KT in the KMN network and disassembling the improperly attached KT–MT fibers (Lampson et al., 2004; Cheeseman and Desai, 2008). Dynein drives the poleward movement of the chromosomes, and CENP-E enables the monooriented chromosome at the pole to glide along the existing K-fiber toward the spindle equator. The unattached KT of the chromosome attaches to the MT that is growing from the opposite pole (Cheeseman and Desai, 2008). When bioriented at the equator, the Ndc80 complex is dephosphorylated to stably attach to the K-fibers. Two phosphatases have been suggested to be involved in chromosome congression: PP1 (Kim et al., 2010; DeLuca et al., 2011) and the B56α subunit of PP2A (Suijkerbuijk et al., 2012; Kruse et al., 2013). We found here that BubR1 acetylation is required to bind PP2A-B56α, suggesting that BubR1 acetylation is a signal cross talking with phosphorylation at the KARD domain at the C terminus (Suijkerbuijk et al., 2012; Kruse et al., 2013) that integrates the phosphatase to the KMN network for chromosome alignment. As the phosphorylation of T680 was not altered but coincided with total BubR1 level in *K243R/+* prometaphase cells, it is possible that sites other than T680 in the KARD domain may be affected by acetylation of BubR1. Or, acetylation may act in concert with all three phosphorylation sites in the KARD domain (Suijkerbuijk et al., 2012; Kruse et al., 2013).

Together, these findings indicate that chromosome congression failure in *K243R/+* cells is a result of the unstable interaction between KT and MT. Malorientation of chromosomes cannot be corrected, and the reduced association of CENP-E at KTs may exacerbate the problem (Fig. 7, left). Future studies should examine whether an acetylation–phosphorylation signaling code in BubR1 is involved in sensing tension and linking it to SAC.

SAC signal establishment was intact in *K243R/+* cells. This signal establishment was also unaffected in haploinsufficient *BubR1* MEFs, indicating that neither reduced BubR1 levels or BubR1 acetylation deficiency affects Mad1/Mad2 localization to the unattached KTs. Blockade of proteolysis led to association of acetylation-deficient BubR1 with other MCC components, similar to WT BubR1. In comparison, the

Published July 22, 2013

Table 4. ***p53* status in *K243R/+* tumors**

Tumor	Sex	Age	Mutation[a]	Mutant[a]	Effect	p_domain[b]
		wk				
Hepatocellular carcinoma 1	Male	61	c.163ins_T	STOP 55	Insertion	TAD
Hepatocellular carcinoma 2	Male	117	c.242C>T	p.A81V	Missense	PRD
			c.301C>T	p.Q101X	Nonsense	DBD
Sarcoma 1	Male	69	c.163ins_T	STOP 55	Insertion	TAD
			c.296ins_A	STOP 99	Insertion	DBD
Sarcoma 2	Female	122	c.296ins_A	STOP 99	Insertion	DBD
			c.467C>T	p.A156V	Missense	DBD
B cell lymphoma 1	Female	62	c.359-365del7	STOP 128	Deletion	DBD
B cell lymphoma 2	Female	119	c.109T>C;980T>C	p.S37P;L327P	Missense	TAD, 4D
			c.429G>A	p.W143X	Nonsense	DBD
B cell lymphoma 3	Female	139	c.443C>T	p.P148L	Missense	DBD
Leukemia 1	Female	57	c.1064A>G	p.E355G	Missense	DBD
			c.841A>G	p.T281A	Missense	DBD

[a]Mutation nomenclatures follow the Human Genome Variation Society recommendations. c, coding sequence; ins, insertion; del, deletion; p, protein sequence. *p53* status was determined by the nucleotide sequencing of four to five clones derived from each tumor.
[b]Protein domain with mutation indicated. TAD, transactivation domain; PRD, proline-rich domain; DBD, DNA-binding domain; 4D, tetramerization domain.

acetylation-deficient BubR1-containing MCC was not intact in Noc-treated MEFs, because of the premature K243R ubiquitination and degradation, which led to premature disassembly of the MCC and consequent failure to sustain the SAC (Fig. 7, right). Thus, the acetylation-deficient *BubR1* allele (*K243R*) functions as a dominant allele both in chromosome–spindle attachment and in SAC maintenance. The fact that both the *K243R* and WT alleles are present in primary tumors of *K243R/+* mice supports this notion (Fig. S3).

The spontaneous tumorigenesis in *K243R/+* mice is because of the dual roles of BubR1 acetylation in mitosis: chromosome–spindle attachment and SAC manintenance. In *K243R/+* cells, malorientated chromosomes are not corrected and before SAC satisfaction, cells proceed through mitosis and produce massive chromosome missegregations.

Chromosome missegregation can give rise to aneuploidy. Although aneuploidy can be oncogenic, this condition can also inhibit growth (Weaver et al., 2007; Sheltzer et al., 2011; Oromendia et al., 2012). Considering that cancers are the result of multiple mutations, the high incidence of spontaneous cancer development in *K243R/+* mice suggests that BubR1 acetylation deficiency not only promotes aneuploidy but also induces multiple genetic changes. General DNA damage, however, was not increased in the *K243R/+* mice, even when compared with Mad2-overexpressing mice (Sotillo et al., 2007). Therefore, it is conceivable to think that chromosome missegregation that results from the failure of chromosome–spindle attachment combined with weakened SAC in *K243R/+* mice yields genetic alterations, in addition to chromosome number instability.

Errors in mitosis and the resulting micronuclei have been suggested by Crasta et al. (2012) as a source of chromothripsis, the shattering of chromosomes and one-off genetic rearrangement in cis (Stephens et al., 2011; Kloosterman et al., 2012). We have not yet analyzed the genome-wide sequencing of tumors to support the idea that chromothripsis accompanies the tumorigenesis in *K243R/+* mice; yet, the signs of chromosome pulverizations with a marked increase of micronuclei from primary cells to tumors suggest the possibility of a chromothripsis-like event taking place in the tumorigenesis of *K243R/+*. A previous paper suggested that *p53* mutation is linked with chromothripsis in sonic hedgehog–associated pediatric medulloblastoma (Rausch et al., 2012). That the *p53* mutation is highly associated with the tumorigenesis of *K243R/+* mice is interesting in this line of thinking.

It is also worth looking into the mutation types we observed in the case of *p53*. As found in *p53*, we propose that small insertions, deletions, and missense mutations can also result from DNA replication–uncoupled micronuclei. As the homozygous mutant mice (*BubR1*$^{K243R/K243R}$) exhibited early embryonic lethality, we propose that the degree of chromosome missegregation in *K243R/+* cells was just enough to be tolerated through embryogenesis but generated a mutation-prone cellular environment that led to tumorigenesis. The accompanying aneuploidy in these cells may have contributed to the process of cancer development.

Lysine 250, which is the acetylation site in human BubR1 (Choi et al., 2009), was also suggested for sumoylation after we reported the acetylation of this site (Yang et al., 2012a). Yang et al. (2012b) proposed that sumoylation occurs after BubR1 deacetylation, suggesting that deacetylation and sumoylation may be involved in mitotic exit. One might argue that the phenotype exhibited in *K250R/+* cells is the result of the combination of acetylation and sumoylation deficiency. We cannot completely rule out this possibility. However, because the consequences of the *K250Q* mutation, which mimics acetylated BubR1, is completely opposite to those observed in *K250R* with respect to the SAC activity and congression, it is more likely that the tumorigenesis stems from the problems in mitosis that resulted from the acetylation deficiency for the following reasons. First, *K250Q* expression rescues the congression defects in BubR1-depleted cells (Fig. 5 E and Fig. S2 A). Second, *K250Q*-expressing cells do not segregate for long (Choi et al., 2009). Finally, *K250Q* expression rescues *BRCA2* deficiency, whereas *K250R* expression does not (Choi et al., 2012).

Published July 22, 2013

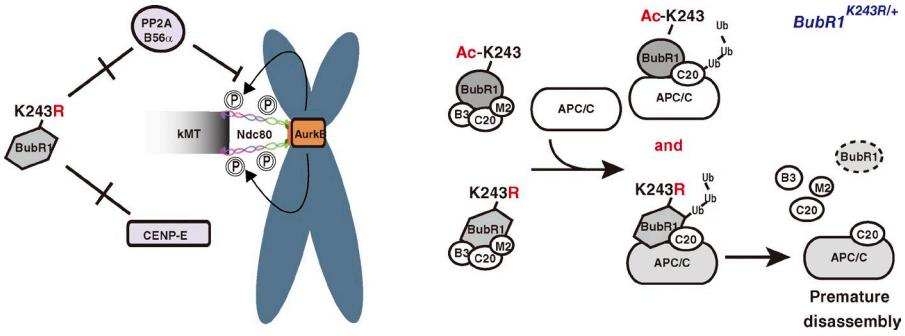

Figure 7. **Model for how tumor develops in *K243R/+* mice.** BubR1 acetylation plays dual roles: it is required for stable maintenance of the KT–MT interaction and for SAC maintenance. *K243R/+* cells exhibit congression failure because 50% of BubR1 is acetylation deficient. Acetylation-deficient BubR1 (K243R) is incapable of recruiting PP2A-B56α to counteract excessive Aurora B kinase activity at the KMN network, and this process is crucial for stable KT–MT interaction. K243R also has reduced CENP-E binding, which may contribute to the problem in chromosome congression (left). Half of the SAC complex contains K243R-BubR1 and fails to maintain SAC activity. K243R associates with other MCC components; however, the protein is readily ubiquitinated by the APC/C, resulting in disassociation of MCC. As initial SAC signal generation is intact, premature disassembly of MCC leads to failure in the maintenance of SAC, effectively weakening SAC activity. The combined effects of chromosome–spindle attachment failure and weakened SAC lead to massive chromosome missegregation and initiate tumorigenesis in *K243R/+* mice.

Although a mutation at K250 in *BubR1* has not been identified in human cancers, it is possible that *BubR1* mutations at sites other than K250 interfere with BubR1 acetylation. Furthermore, the *BRCA2* tumor suppressor is required for BubR1 acetylation during mitosis (Choi et al., 2012). We proposed that BRCA2, which is a regulator of mitosis but not a critical component of the SAC, may be the preferred target in tumorigenesis (Choi et al., 2012). The analysis of the *K243R/+* mice suggests that BubR1 acetylation is indeed a tumor-suppressive mechanism.

Materials and methods

Generation of the BubR1 acetylation-deficient (K243R) allele and *BubR1$^{K243R/+}$; GFP-H2B* mice

Mouse *BubR1* genomic DNA was isolated by screening the mouse 129/Sv library (Agilent Technologies) using a probe from mouse *BubR1* cDNA, and two BAC clones were mapped and sequenced. To generate the targeting vector, an 8-kb fragment containing exons 5, 6, 7, and 8 was cloned into the pBluescript KS (+) vector. The neo cassette and diphtheria toxin A fragment were also inserted into the vector (Fig. 1). The lysine at position 243 in *BubR1* was substituted with an arginine using site-directed mutagenesis in the targeting construct. The targeting construct was linearized and electroporated into 129/Sv embryonic stem (ES) cells. The accurately targeted ES cell clones were selected using Southern blotting and DNA sequencing analysis. The heterozygous ES cells were injected into the blastocysts of C57BL/6 mice to generate the *K243R/+* mice. The neo cassette was removed by crossing the *K243R/+* mice with *Flpe* transgenic mice. The primers used for PCR genotyping were as follows: 5′-GAGGTAAAGGCAGGGGAATC-3′ (forward) and 5′-GAGAAAGCGGGGGTCATTAT-3′ (reverse).

The *K243R/+* mice were crossed with *EGFP-H2B* transgenic mice (B6.Cg-Tg[HIST1H2BB/EGFP]1 pa/J; The Jackson Laboratory) for monitoring cell division. The *BubR1$^{+/-}$* mice were a gift from W. Dai (New York University School of Medicine, Tuxedo, NY). The mice were housed in a specific pathogen-free facility or semi-conventional (virus antibody–free) facility. The Institutional Animal Care and Use Committee of Seoul National University (SNU-090630-3) approved the animal experimental protocols. The guidelines, policies, and regulations for the Care and Use of Laboratory Animals in Seoul National University were followed.

Genotyping

PCR was used to genotype the adult BubR1 acetylation-deficient mice using genomic DNA extracted from the tail. The genomic DNA from the in vitro cultured ES cells and embryos was extracted using the DirectPCR reagent (Viagen Biotech, Inc.). A 3–5-µl sample of the genomic DNA was used for the PCR. The primers for BubR1 were as follows: 5′-CCCTCACAAACGCCTACC-3′ (forward) and 5′-CATCTCACCAGCCCAGAAGA-3′ (reverse). The resulting PCR products were separated on a 1.5% agarose gel. Using the primers indicated, the WT DNA produced a 145-bp PCR product, and the homozygote mutant allele produced a slower migrating 219-bp band. We verified the PCR genotyping by sequencing of the targeted region. The sequencing primers used were as follows: 5′-GGTTGTCCTTTGTCTTGCT-3′ and 5′-TGCTTACCATCTCTTGGGT-3′ for reverse sequence confirmation.

Statistical analysis

The relationships between categorical variables were assessed using the χ^2 test. Tumor- and cancer-free survival were estimated using the Kaplan-Meier method. For the statistical analyses, *t* test was used unless otherwise stated. The means ± SEM or SD are shown. The statistical data were analyzed using SPSS software (version 15.0; SPSS Inc.).

Embryo culture

E3.5 blastocysts from intercrosses of the *K243R/+* mice were harvested into gelatinized 4-well plates. The embryos were cultured in DMEM supplemented with 1,000 U/ml leukemia inhibitor factor (ESGRO), 15% vol/vol FBS, 100 mM sodium pyruvate, 10,000 U/ml of penicillin, 10,000 µg/ml of streptomycin, 200 mM L-glutamine, 100 µM MEM nonessential amino acids, and 55 µM β-mercaptoethanol for 6 d. The embryos were examined using a phase-contrast microscope (Axio Observer.Z1; Carl Zeiss) before genotyping.

Constructs and antibodies

PP2A-B56α-expressing constructs were gifts from G. Kops (University Medical Center, Utrecht, Netherlands) and J. Nilsson (University of Copenhagen, Copenhagen, Denmark). *EGFP-PP2A-B56α*–expressing construct was generated by subcloning *PP2A-B56α* into EGFP-N1 vector (Invitrogen). The following antibodies were used: anti-cyclin A (H-432), anti–cyclin B (H-433), anti-Mad2 (C-19), anti-PCAF (H369 and E-8), anti-CDC20 (H-175), and anti-APC3 (Santa Cruz Biotechnology, Inc.); anti–α-tubulin (DM1A), anti–γ-tubulin, and anti-actin (AC-15; Sigma-Aldrich); anti-BubR1 and anti–PP2A-B56α (BD); anti–phospho-histone H3, anti–acetyl-lysine monoclonal, and anti–γ-H2AX (EMD Millipore); CREST (Cortex Biochem); anti-CD3 (2C11) and anti-B220 (RA3-6B2; BioLegend); anti–von Willebrand factor and anti–Ki-67 (Dako); anti–acetyl-lysine polyclonal (Cell Signaling Technology); Alexa Fluor 488–phalloidin (Invitrogen); and Alexa Fluor 488 goat anti–mouse IgG (Molecular Probes). The anti-Bub3 antibody was a gift from S. Taylor (University of Manchester, Manchester, UK). The anti-Mad2 and anti-Mad1 antibodies were obtained from H. Yu (University of Texas Southwestern Medical Center, Dallas, TX) and the anti-Blinkin antibody was obtained from I. Cheeseman (Whitehead Institute for Biomedical Research, Cambridge, MA). The anti–phospho-Hec1 antibody was obtained from J. Deluca (Colorado State University, Fort Collins, CO), the anti-pT680 antibody from G. Kops, and the anti–CENP-E (Hpx-1) antibody from D. Cleveland (University of California Ludwig Institute, San Diego, CA).

Stable inducible HeLa-FRT cell lines, transfection, and depletion of endogenous BubR1

The WT *hBubR1* was cloned into pcDNA5/FRT/TO (a gift from J. Pines, Gurdon Institute, Cambridge, UK), and mutagenesis was performed to generate *BubR1-K250R* and *-K250Q* mutants. The HeLa-FRT/TO cells (a gift from S. Taylor) were cotransfected with the pOG44 and pcDNA5/FRT/TO-BubR1 constructs, and the cells were selected according to the FLIP-in protocol (Invitrogen). The *PP2A-B56α*–expressing HeLa-FRT/TO cell line

Published July 22, 2013

was a gift from J. Nilsson. HeLa-FRT stable cells were treated with 1 µg/ml of doxycycline to induce expression of *BubR1* mutants or *PP2A-B56α*, followed by treatment with 200 ng/ml Noc and 10 µM MG132 to enrich cells in mitosis. Cell lysates were subjected to IP and WB.

IP and WB analysis

Cells were lysed in NETN buffer (150 mM NaCl, 1 mM EDTA, 20 mM Tris, pH 8.0, and 0.5% NP-40) supplemented with protease inhibitors for IP and WB analysis. The mouse tissues were resuspended in lysis buffer (1% Triton X-100, 150 mM NaCl, 50 mM Tris, pH 8.0, and 1 mM EGTA) plus the complete EDTA-free proteinase inhibitor cocktail (Roche), which was dissolved in PBS, pH 7.4, and homogenized. For detection of the acetylated BubR1, 20 µM of trichostatin A was added to the NETN buffer.

Immunofluorescence assay

The immunofluorescence assays were performed as previously described with slight modifications for staining the paraffin-embedded tissues (Choi and Lee, 2008; Choi et al., 2009, 2012). In brief, cells were grown on coverslips, fixed in 4% paraformaldehyde, and permeabilized by two incubations in PBS-0.5% Triton X-100 (0.5% PBST) for 15 min at RT before being subjected to indirect immunofluorescence microscopy. Goat serum (20%) in 0.1% PBST was used as the blocking agent and the antibody dilution solution. After permeabilization, the fixed cells were incubated in blocking buffer for 1 h at RT. The cells were incubated with the indicated primary antibodies for 1 h at RT or overnight at 4°C followed by incubation with fluorescence-conjugated secondary antibodies.

Histopathology

Tissue specimens were collected from all organs that exhibited an abnormal appearance. Hematoxylin and eosin (H&E) staining was conducted following the standard procedures. First, paraffinized tissue block was deparaffinization in xylene, followed by rehydration in ethanol in a serial manner (100%, 95%, and 70%), and subjected to hematoxylin staining. Then the specimen was decolorized in acid alcohol and counterstained with eosin. H&E or immunohistochemical stains and were reviewed by the pathologist (G. Gong). The immunohistochemical analyses were performed as previously described with slight modifications (Lee et al., 2009). The sections were incubated with an anti-B220 antibody at a 1:100 dilution in a humidifying chamber at 4°C overnight.

Cytogenetics

For metaphase spreads, MEFs and lymphocytes were treated with 0.1 and 10 µg/ml colcemid for 7 and 2 h, respectively, and were collected by centrifugation. The cells were incubated in a hypotonic solution (0.075 M KCl) for 20 min at 37°C and were centrifuged slowly at 800 rpm for 5 min. The supernatant was removed, and the cells were rinsed once with fixation solution (methanol/acetic acid = 3:1). The cells were incubated in fixation solution overnight at 4°C and placed onto humidified, clean glass slides in a 65°C water bath. The slides were dried and stained in 5% Giemsa solution (Gibco) in phosphate buffer, pH 6.8. The stained slides were mounted with glycerol and were examined under a light microscope (Axio Imager. A1; Carl Zeiss). For the SKY analysis, the *K243R/+* MEFs (at passage 27) were treated with 5 µg/ml colcemid for 7 h before fixation. The SKY analysis was performed at the Molecular Cytogenetics Core at the University of Texas M.D. Anderson Cancer Center.

For chromosome spreads coupled with immunofluorescence assays, the basic protocol by Choi et al. (2012) was followed, except that cells were incubated with 200 ng/ml Noc for 4 h instead of with colcemid. Cells were swelled in tap water and cytospinned at 850 rpm for 5 min. The slides were subjected to immunofluorescence assay as described.

Mitotic index measurements in MEFs

The cells were fixed in cold 70% ethanol overnight. The fixed cells were incubated for 1 h at RT with MPM2 antibodies (EMD Millipore) diluted in PBS, 0.02% Triton X-100, and 2% BCS. The cells were washed twice in PBS and incubated with Alexa Fluor 488–conjugated goat anti–mouse antibody (Molecular Probes) for 1 h at RT. The cells were treated with RNase, and the DNA was stained with 7-amino-actinomycid D or propidium iodide and analyzed in a FACS Canto machine (BD).

Partial hepatectomy

10–15-wk-old mice were anesthetized using a mixture of isoflurane/oxygen, and a 70% partial hepatectomy and excision of the medial and left lateral lobes was performed (Mitchell and Willenbring, 2008). At least three animals were used for each time point. After the procedure, the mice were maintained in ad libitum conditions and were killed by cervical dislocation at the indicated time points. The livers were harvested and processed for subsequent analyses.

Microscope image acquisition and processing

Fixed cell images were acquired with a microscope (DeltaVision; Applied Precision) equipped with a 100× objective lens (Olympus). The images were obtained with 0.2-µm-distanced optical sections in z-axis. Each section was deconvoluted and projected into one image using the softWoRx software (Applied Precision) for image display.

For live-cell imaging, cells were monitored using the UPlanFL N 40×/NA 1.30 oil lens on a microscope (DeltaVision Cpre; GE Healthcare) equipped with a charge-coupled device camera (Photometrics) in a CO_2 chamber at 37°C (Applied Precision) as previously described (Choi and Lee, 2008; Choi et al., 2009). The cells were seeded in a glass-bottom dish containing DMEM supplemented with 20% FBS and 2 mM L-glutamine and analyzed after 6 h. The images were acquired every 5 min using a 20× objective lens (Olympus).

Cold stable MT assay and scoring of the immunofluorescence intensity

The cells were treated with 10 µM MG132 for 2 h and incubated with serum-free DMEM containing 20 mM Hepes, pH 7.3, for 10 min on ice. When cold MT assay was performed to assess recovery from Monastrol treatment, cells were treated with 100 µM Monastrol for 3 h. In the final hour, cells were incubated with 10 µM MG132 as well. Monastrol-arrested cells were washed at least three times with fresh media containing 10 µM MG132. The cells were released into media with 10 µM MG132 for 1 h. The cells were fixed in 4% paraformaldehyde for 10 min and the immunofluorescence assays were performed as needed.

Images were acquired and processed using DetaVision Softworx software (GE Healthcare), and the images for display were generated by projecting the sum of the optical sections. Quantitative analysis of the immunofluorescence was performed in the projected images using the Image J software (National Institutes of Health). For quantification of intensities at KTs, a mask covering each KT foci was created within a circular region, and the mean pixel intensities were obtained. More than 300 KTs were scored for the intensities in each experiment for statistical analysis.

Mutation analysis of *p53* in tumors

The total RNA was extracted from the tumors using the TRIzol reagent (Invitrogen), and the cDNA was synthesized using Superscript II reverse transcription (Invitrogen). The PCR primers were designed to cover the entire mouse p53 sequence as follows: 5′-ATGGAGGAGTCACAGTCGGATATC-3′ (forward) and 5′-TCAGTCTGAGTCAGGCCCC-3′ (reverse). The *p53* status was analyzed by the nucleotide sequencing of at least four clones derived from each tumor.

Online supplemental material

Fig. S1 shows that there is no difference in *BubR1* expression in the thymus and testis, as well as body weight change between *K243R/+* and WT mice. Fig. S2 shows that BubR1 acetylation is involved in proper chromosome congression. Fig. S3 shows that both WT *BubR1* and *K243R-BubR1* alleles are detected in *K243R/+* primary tumors by PCR. Videos related to Fig. 4 G are also available: Video 1 is the live imaging of mitosis in WT MEFs and Videos 2 and 3 are the live imaging of *K243R/+* MEFs. Online supplemental material is available at http://www.jcb.org/cgi/content/full/jcb.201210099/DC1. Additional data are available in the JCB DataViewer at http://dx.doi.org/10.1083/jcb.201210099.dv.

Animal care and breeding were carried out in the Specific Pathogen Free Mouse Facility of Seoul National University. Imaging and flow cytometry analysis were carried out at the Institute of Molecular Biology and Genetics Imaging Facility. We are very grateful to W. Dai for generously providing the *BubR1*$^{+/-}$ mice. We thank H.S. Min for the help with several of the pathological analyses. We thank D. Cleveland, J. Deluca, J. Nilsson, G. Kops, J. Pines, H. Yu, S. Taylor, and I. Cheeseman for valuable reagents.

The Basic Science Research Program (2008-0059996), the Novel Drug Target Validation by the Korean National Research Foundation (2012M3A9A8052), and the Cancer Control Program of the Korean Ministry of Health (1220210) funded this research.

Submitted: 19 October 2012
Accepted: 12 June 2013

Published July 22, 2013

References

Abrieu, A., J.A. Kahana, K.W. Wood, and D.W. Cleveland. 2000. CENP-E as an essential component of the mitotic checkpoint in vitro. *Cell*. 102:817–826. http://dx.doi.org/10.1016/S0092-8674(00)00070-2

Baker, D.J., K.B. Jeganathan, J.D. Cameron, M. Thompson, S. Juneja, A. Kopecka, R. Kumar, R.B. Jenkins, P.C. de Groen, P. Roche, and J.M. van Deursen. 2004. BubR1 insufficiency causes early onset of aging-associated phenotypes and infertility in mice. *Nat. Genet.* 36:744–749. http://dx.doi.org/10.1038/ng1382

Bolanos-Garcia, V.M., T. Lischetti, D. Matak-Vinković, E. Cota, P.J. Simpson, D.Y. Chirgadze, D.R. Spring, C.V. Robinson, J. Nilsson, and T.L. Blundell. 2011. Structure of a Blinkin-BUBR1 complex reveals an interaction crucial for kinetochore-mitotic checkpoint regulation via an unanticipated binding Site. *Structure*. 19:1691–1700. http://dx.doi.org/10.1016/j.str.2011.09.017

Chan, G.K., S.A. Jablonski, V. Sudakin, J.C. Hittle, and T.J. Yen. 1999. Human BUBR1 is a mitotic checkpoint kinase that monitors CENP-E functions at kinetochores and binds the cyclosome/APC. *J. Cell Biol.* 146:941–954. http://dx.doi.org/10.1083/jcb.146.5.941

Cheeseman, I.M., and A. Desai. 2008. Molecular architecture of the kinetochore-microtubule interface. *Nat. Rev. Mol. Cell Biol.* 9:33–46. http://dx.doi.org/10.1038/nrm2310

Cheeseman, I.M., J.S. Chappie, E.M. Wilson-Kubalek, and A. Desai. 2006. The conserved KMN network constitutes the core microtubule-binding site of the kinetochore. *Cell*. 127:983–997. http://dx.doi.org/10.1016/j.cell.2006.09.039

Choi, E., and H. Lee. 2008. Chromosome damage in mitosis induces BubR1 activation and prometaphase arrest. *FEBS Lett.* 582:1700–1706. http://dx.doi.org/10.1016/j.febslet.2008.04.028

Choi, E., H. Choe, J. Min, J.Y. Choi, J. Kim, and H. Lee. 2009. BubR1 acetylation at prometaphase is required for modulating APC/C activity and timing of mitosis. *EMBO J.* 28:2077–2089. http://dx.doi.org/10.1038/emboj.2009.123

Choi, E., P.G. Park, H.O. Lee, Y.K. Lee, G.H. Kang, J.W. Lee, W. Han, H.C. Lee, D.Y. Noh, S. Lekomtsev, and H. Lee. 2012. BRCA2 fine-tunes the spindle assembly checkpoint through reinforcement of BubR1 acetylation. *Dev. Cell*. 22:295–308. http://dx.doi.org/10.1016/j.devcel.2012.01.009

Crasta, K., N.J. Ganem, R. Dagher, A.B. Lantermann, E.V. Ivanova, Y. Pan, L. Nezi, A. Protopopov, D. Chowdhury, and D. Pellman. 2012. DNA breaks and chromosome pulverization from errors in mitosis. *Nature*. 482:53–58. http://dx.doi.org/10.1038/nature10802

De Antoni, A., C.G. Pearson, D. Cimini, J.C. Canman, V. Sala, L. Nezi, M. Mapelli, L. Sironi, M. Faretta, E.D. Salmon, and A. Musacchio. 2005. The Mad1/Mad2 complex as a template for Mad2 activation in the spindle assembly checkpoint. *Curr. Biol.* 15:214–225. http://dx.doi.org/10.1016/j.cub.2005.01.038

DeLuca, J.G., W.E. Gall, C. Ciferri, D. Cimini, A. Musacchio, and E.D. Salmon. 2006. Kinetochore microtubule dynamics and attachment stability are regulated by Hec1. *Cell*. 127:969–982. http://dx.doi.org/10.1016/j.cell.2006.09.047

DeLuca, K.F., S.M. Lens, and J.G. DeLuca. 2011. Temporal changes in Hec1 phosphorylation control kinetochore-microtubule attachment stability during mitosis. *J. Cell Sci.* 124:622–634. http://dx.doi.org/10.1242/jcs.072629

Guo, Y., C. Kim, S. Ahmad, J. Zhang, and Y. Mao. 2012. CENP-E–dependent BubR1 autophosphorylation enhances chromosome alignment and the mitotic checkpoint. *J. Cell Biol.* 198:205–217. http://dx.doi.org/10.1083/jcb.201202152

Hao, X., M.S. Shin, J.X. Zhou, C.H. Lee, C.F. Qi, Z. Naghashfar, J.W. Hartley, T.N. Fredrickson, J.M. Ward, and H.C. Morse III. 2006. Histologic and molecular characterizations of megakaryocytic leukemia in mice. *Leuk. Res.* 30:397–406. http://dx.doi.org/10.1016/j.leukres.2005.08.021

Johnson, V.L., M.I. Scott, S.V. Holt, D. Hussein, and S.S. Taylor. 2004. Bub1 is required for kinetochore localization of BubR1, Cenp-E, Cenp-F and Mad2, and chromosome congression. *J. Cell Sci.* 117:1577–1589. http://dx.doi.org/10.1242/jcs.01006

Kapoor, T.M., M.A. Lampson, P. Hergert, L. Cameron, D. Cimini, E.D. Salmon, B.F. McEwen, and A. Khodjakov. 2006. Chromosomes can congress to the metaphase plate before biorientation. *Science*. 311:388–391. http://dx.doi.org/10.1126/science.1122142

Kim, S., and H. Yu. 2011. Mutual regulation between the spindle checkpoint and APC/C. *Semin. Cell Dev. Biol.* 22:551–558. http://dx.doi.org/10.1016/j.semcdb.2011.03.008

Kim, Y., A.J. Holland, W. Lan, and D.W. Cleveland. 2010. Aurora kinases and protein phosphatase 1 mediate chromosome congression through regulation of CENP-E. *Cell*. 142:444–455. http://dx.doi.org/10.1016/j.cell.2010.06.039

Kiyomitsu, T., C. Obuse, and M. Yanagida. 2007. Human Blinkin/AF15q14 is required for chromosome alignment and the mitotic checkpoint through direct interaction with Bub1 and BubR1. *Dev. Cell*. 13:663–676. http://dx.doi.org/10.1016/j.devcel.2007.09.005

Kloosterman, W.P., M. Tavakoli-Yaraki, M.J. van Roosmalen, E. van Binsbergen, I. Renkens, K. Duran, L. Ballarati, S. Vergult, D. Giardino, K. Hansson, et al. 2012. Constitutional chromothripsis rearrangements involve clustered double-stranded DNA breaks and nonhomologous repair mechanisms. *Cell Rep.* 1:648–655. http://dx.doi.org/10.1016/j.celrep.2012.05.009

Kruse, T., G. Zhang, M.S. Larsen, T. Lischetti, W. Streicher, T. Kragh Nielsen, S.P. Bjørn, and J. Nilsson. 2013. Direct binding between BubR1 and B56-PP2A phosphatase complexes regulate mitotic progression. *J. Cell Sci.* 126:1086–1092. http://dx.doi.org/10.1242/jcs.122481

Lampson, M.A., and I.M. Cheeseman. 2011. Sensing centromere tension: Aurora B and the regulation of kinetochore function. *Trends Cell Biol.* 21:133–140. http://dx.doi.org/10.1016/j.tcb.2010.10.007

Lampson, M.A., and T.M. Kapoor. 2005. The human mitotic checkpoint protein BubR1 regulates chromosome-spindle attachments. *Nat. Cell Biol.* 7:93–98. http://dx.doi.org/10.1038/ncb1208

Lampson, M.A., K. Renduchitala, A. Khodjakov, and T.M. Kapoor. 2004. Correcting improper chromosome-spindle attachments during cell division. *Nat. Cell Biol.* 6:232–237. http://dx.doi.org/10.1038/ncb1102

Lara-Gonzalez, P., F.G. Westhorpe, and S.S. Taylor. 2012. The spindle assembly checkpoint. *Curr. Biol.* 22:R966–R980. http://dx.doi.org/10.1016/j.cub.2012.10.006

Lee, Y.K., E. Choi, M.A. Kim, P.G. Park, N.H. Park, and H. Lee. 2009. BubR1 as a prognostic marker for recurrence-free survival rates in epithelial ovarian cancers. *Br. J. Cancer*. 101:504–510. http://dx.doi.org/10.1038/sj.bjc.6605161

Malureanu, L.A., K.B. Jeganathan, M. Hamada, L. Wasilewski, J. Davenport, and J.M. van Deursen. 2009. BubR1 N terminus acts as a soluble inhibitor of cyclin B degradation by APC/C(Cdc20) in interphase. *Dev. Cell*. 16:118–131. http://dx.doi.org/10.1016/j.devcel.2008.11.004

Mao, Y., A. Abrieu, and D.W. Cleveland. 2003. Activating and silencing the mitotic checkpoint through CENP-E-dependent activation/inactivation of BubR1. *Cell*. 114:87–98. http://dx.doi.org/10.1016/S0092-8674(03)00475-6

Michel, L.S., V. Liberal, A. Chatterjee, R. Kirchwegger, B. Pasche, W. Gerald, M. Dobles, P.K. Sorger, V.V. Murty, and R. Benezra. 2001. MAD2 haploinsufficiency causes premature anaphase and chromosome instability in mammalian cells. *Nature*. 409:355–359. http://dx.doi.org/10.1038/35053094

Mitchell, C., and H. Willenbring. 2008. A reproducible and well-tolerated method for 2/3 partial hepatectomy in mice. *Nat. Protoc.* 3:1167–1170. http://dx.doi.org/10.1038/nprot.2008.80

Oromendia, A.B., S.E. Dodgson, and A. Amon. 2012. Aneuploidy causes proteotoxic stress in yeast. *Genes Dev.* 26:2696–2708. http://dx.doi.org/10.1101/gad.207407.112

Rausch, T., D.T. Jones, M. Zapatka, A.M. Stütz, T. Zichner, J. Weischenfeldt, N. Jäger, M. Remke, D. Shih, P.A. Northcott, et al. 2012. Genome sequencing of pediatric medulloblastoma links catastrophic DNA rearrangements with TP53 mutations. *Cell*. 148:59–71. http://dx.doi.org/10.1016/j.cell.2011.12.013

Rieder, C.L. 1981. The structure of the cold-stable kinetochore fiber in metaphase PtK1 cells. *Chromosoma*. 84:145–158. http://dx.doi.org/10.1007/BF00293368

Rivera, T., and A. Losada. 2009. Shugoshin regulates cohesion by driving relocalization of PP2A in *Xenopus* extracts. *Chromosoma*. 118:223–233. http://dx.doi.org/10.1007/s00412-008-0190-4

Sheltzer, J.M., H.M. Blank, S.J. Pfau, Y. Tange, B.M. George, T.J. Humpton, I.L. Brito, Y. Hiraoka, O. Niwa, and A. Amon. 2011. Aneuploidy drives genomic instability in yeast. *Science*. 333:1026–1030. http://dx.doi.org/10.1126/science.1206412

Sotillo, R., E. Hernando, E. Díaz-Rodríguez, J. Teruya-Feldstein, C. Cordón-Cardo, S.W. Lowe, and R. Benezra. 2007. Mad2 overexpression promotes aneuploidy and tumorigenesis in mice. *Cancer Cell*. 11:9–23. http://dx.doi.org/10.1016/j.ccr.2006.10.019

Stephens, P.J., C.D. Greenman, B. Fu, F. Yang, G.R. Bignell, L.J. Mudie, E.D. Pleasance, K.W. Lau, D. Beare, L.A. Stebbings, et al. 2011. Massive genomic rearrangement acquired in a single catastrophic event during cancer development. *Cell*. 144:27–40. http://dx.doi.org/10.1016/j.cell.2010.11.055

Sudakin, V., G.K. Chan, and T.J. Yen. 2001. Checkpoint inhibition of the APC/C in HeLa cells is mediated by a complex of BUBR1, BUB3, CDC20, and MAD2. *J. Cell Biol.* 154:925–936. http://dx.doi.org/10.1083/jcb.200102093

Suijkerbuijk, S.J., M. Vleugel, A. Teixeira, and G.J. Kops. 2012. Integration of kinase and phosphatase activities by BUBR1 ensures formation of stable

kinetochore-microtubule attachments. *Dev. Cell*. 23:745–755. http://dx.doi.org/10.1016/j.devcel.2012.09.005

Sundin, L.J., and J.G. Deluca. 2010. Kinetochores: NDC80 toes the line. *Curr. Biol.* 20:R1083–R1085. http://dx.doi.org/10.1016/j.cub.2010.11.033

Tang, Z., H. Shu, W. Qi, N.A. Mahmood, M.C. Mumby, and H. Yu. 2006. PP2A is required for centromeric localization of Sgo1 and proper chromosome segregation. *Dev. Cell*. 10:575–585. http://dx.doi.org/10.1016/j.devcel.2006.03.010

Wang, Q., T. Liu, Y. Fang, S. Xie, X. Huang, R. Mahmood, G. Ramaswamy, K.M. Sakamoto, Z. Darzynkiewicz, M. Xu, and W. Dai. 2004. BUBR1 deficiency results in abnormal megakaryopoiesis. *Blood*. 103:1278–1285. http://dx.doi.org/10.1182/blood-2003-06-2158

Weaver, B.A., Z.Q. Bonday, F.R. Putkey, G.J. Kops, A.D. Silk, and D.W. Cleveland. 2003. Centromere-associated protein-E is essential for the mammalian mitotic checkpoint to prevent aneuploidy due to single chromosome loss. *J. Cell Biol.* 162:551–563. http://dx.doi.org/10.1083/jcb.200303167

Weaver, B.A., A.D. Silk, C. Montagna, P. Verdier-Pinard, and D.W. Cleveland. 2007. Aneuploidy acts both oncogenically and as a tumor suppressor. *Cancer Cell*. 11:25–36. http://dx.doi.org/10.1016/j.ccr.2006.12.003

Wei, R.R., J. Al-Bassam, and S.C. Harrison. 2007. The Ndc80/HEC1 complex is a contact point for kinetochore-microtubule attachment. *Nat. Struct. Mol. Biol.* 14:54–59. http://dx.doi.org/10.1038/nsmb1186

Welburn, J.P., M. Vleugel, D. Liu, J.R. Yates III, M.A. Lampson, T. Fukagawa, and I.M. Cheeseman. 2010. Aurora B phosphorylates spatially distinct targets to differentially regulate the kinetochore-microtubule interface. *Mol. Cell*. 38:383–392. http://dx.doi.org/10.1016/j.molcel.2010.02.034

Yang, F., L. Hu, C. Chen, J. Yu, C.B. O'Connell, A. Khodjakov, M. Pagano, and W. Dai. 2012a. BubR1 is modified by sumoylation during mitotic progression. *J. Biol. Chem.* 287:4875–4882. http://dx.doi.org/10.1074/jbc.M111.318261

Yang, F., Y. Huang, and W. Dai. 2012b. Sumoylated BubR1 plays an important role in chromosome segregation and mitotic timing. *Cell Cycle*. 11:797–806.

Published July 22, 2013

Park et al., http://www.jcb.org/cgi/content/full/jcb.201210099/DC1

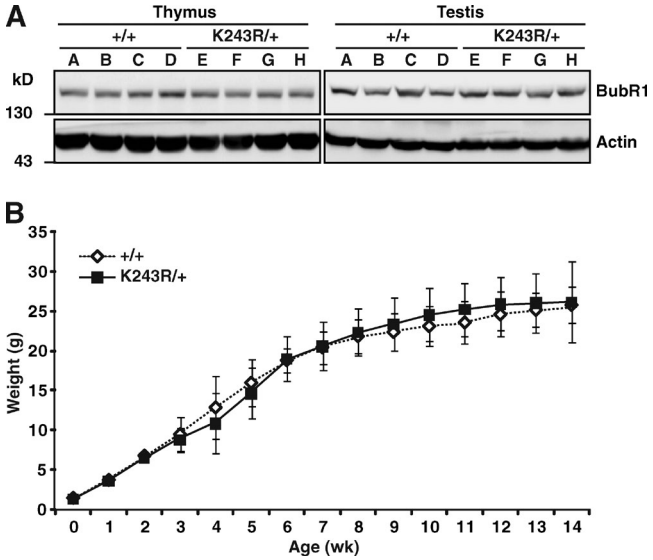

Figure S1. **Analysis of *K243R/+* knock-in mice.** (A) WB analysis of BubR1 protein levels in the thymus and testis. (B) Body weight analysis of WT ($n = 50$) and *K243R/+* ($n = 130$). SDs are shown in error bars.

Published July 22, 2013

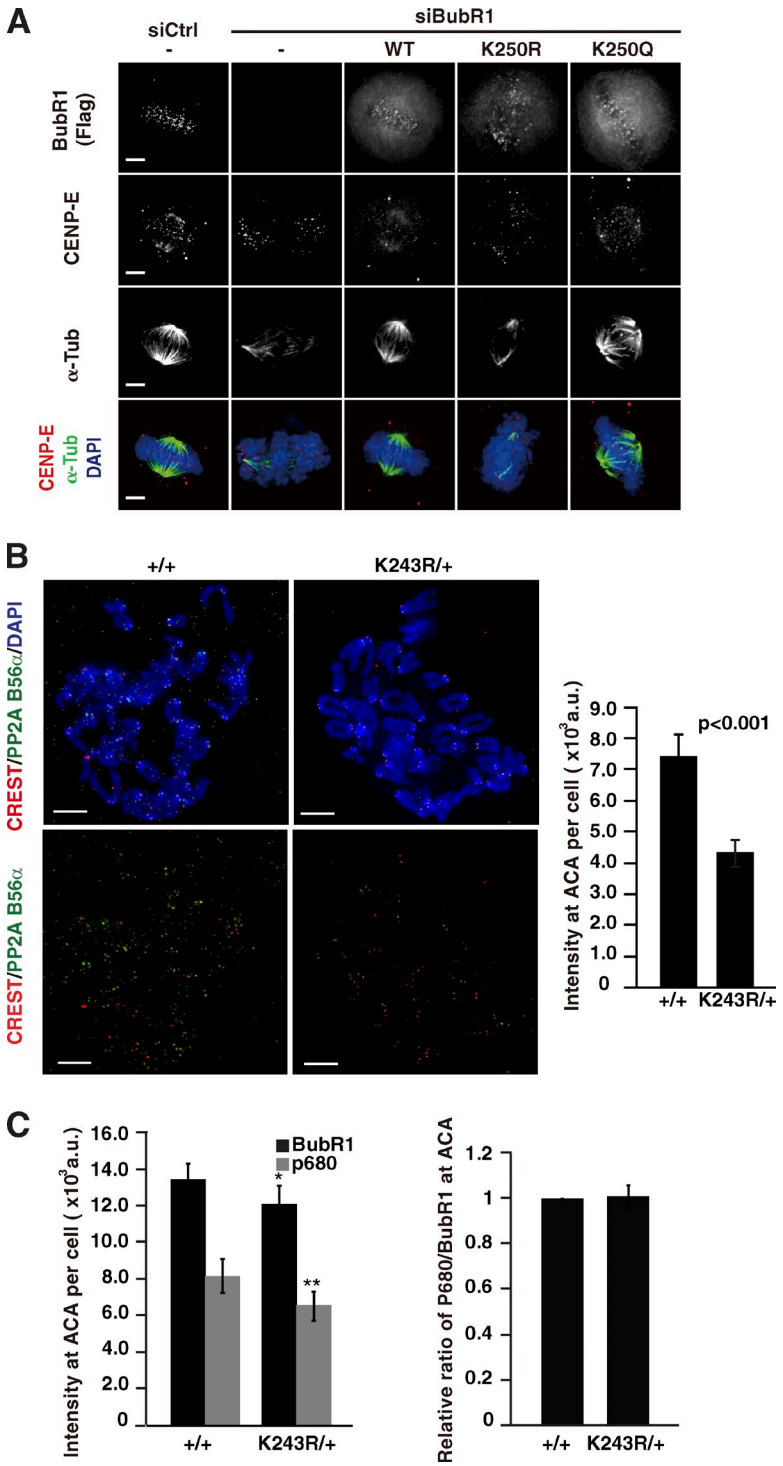

Figure S2. **BubR1 acetylation is involved in proper chromosome congression.** (A) Acetylation-mimetic form of BubR1 (K250Q) is capable of rescuing the defects of KT–MT interaction in BubR1-depleted cells. Hela-FRT-BubR1, -K250R, or -K250Q cells were depleted of endogenous BubR1 by siRNA transfection targeting 3′-UTR. The expression of indicated FLAG-tagged BubR1 constructs was induced by doxycycline treatment. Then they were subjected to cold MT assay after treating cells with MG132 for 1 h. Immunofluorescence assay was performed with anti-BubR1 or anti-FLAG (M2), anti–CENP-E, and anti-tubulin antibodies. Representative metaphase cells are shown (siCtrl, *n* = 11; siBubR1, *n* = 15; siBubR1 + WT, *n* = 10; siBubR1 + K250R, *n* = 15; siBubR1 + K250Q, *n* = 12). Bars, 5 µm. (B) PP2A-B56α recruitment to KTs in WT and *K243R/+* MEFs. Metaphase chromosome spreads were coupled with immunofluorescence assay. Immunofluorescence assay was performed with anti-CREST and anti–PP2A-B56α. The result is from two independent experiments of 27 cells in each setting (mean ± SEM; *n* > 450 KTs). Bars, 5 µm. (C) Relative intensity of p680 BubR1 at KTs of prometaphase cells. MEFs were treated with 200 ng/ml nocodazole and 10 µM Mg132 for 2 h before fixation. Immunofluorescence assay was performed with anti-CREST, anti-pT680 BubR1, and anti-BubR1 antibodies. The result is from two independent experiments of 37 cells in each setting (mean ± SEM; *n* > 350 KTs). Asterisks mark significant p-values calculated by an unpaired *t* test (*, P = 0.32; **, P = 0.18). (right) Relative ratio of p680/BubR1 immunofluorescence intensities are depicted as histograms (SDs are from two independent experiments).

Published July 22, 2013

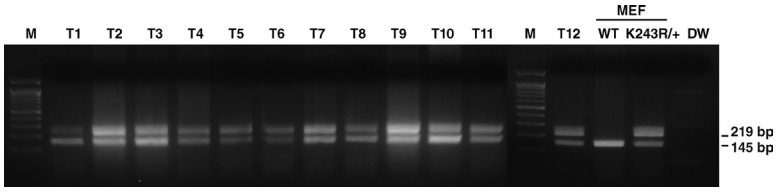

Figure S3. **Detection of WT and K243R allele in primary tumors.** PCR genotyping of *WT-BubR1* and *K243R* from 12 primary tumors obtained from the *K243R/+* mice. Genomic DNA samples from the WT and *K243R/+* MEFs served as the PCR controls.

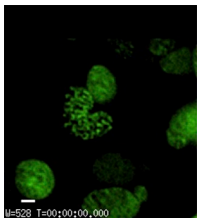

Video 1. **Live imaging of mitosis in WT MEFs.** MEFs isolated from the mice expressing *GFP-H2B* (i.e., GFP-H2B transgenic mice) were subjected to time-lapse video microscopy using the UPlanFL N 40×/NA 1.30 oil lens on a microscope (DeltaVision Cpre) equipped with a charge-coupled device camera in a CO_2 chamber at 37°C. The images were captured every 5 min using a 20× objective lens. Bar, 5 µm.

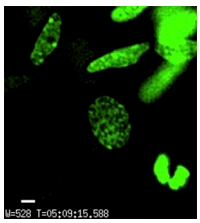

Video 2. **Mitosis in *K243R/+; GFP-H2B* MEFs.** The *GFP-H2B* transgenic mice were crossed with *K243R/+* mice, and the MEFs isolated from the resultant *K243R/+; GFP-H2B* mice were subjected to live imaging as in Video 1. The images were taken every 5 min. The chromosomes segregated without forming distinct metaphase plates. Lagging chromosomes are shown. Bar, 5 µm.

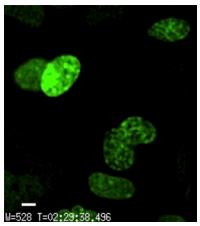

Video 3. **Mitosis in *K243R/+; GFP-H2B* MEFs.** The *GFP-H2B* transgenic mice were crossed with *K243R/+* mice, and the MEFs isolated from the resultant *K243R/+; GFP-H2B* mice were subjected to live imaging as in Video 1. The cells exited mitosis without chromosome segregation. The images were captured every 5 min. Bar, 5 µm.